University of Alberta

Characterization of natural zeolite membranes for H_2/CO_2 separations by single gas permeation

by

Sayed Alireza Hoseinzadeh Hejazi

A thesis submitted to the Faculty of Graduate Studies and Research
in partial fulfillment of the requirements for the degree of

Master of Science
in
Chemical Engineering

Department of Chemical and Materials Engineering

Fall 2011
Edmonton, Alberta

Dedicated to my parents

Abstract

Membrane-based processes have the potential to overcome the limitations of conventional hydrogen separation techniques such as high energy consumption and environmental concerns. Natural zeolite membranes have recently been shown to demonstrate apparent molecular sieving of H_2 from H_2/CO_2 mixtures and can be used as a model for the development of robust molecular sieve membranes with superior separation characteristics.

The focus of this thesis is the characterization of natural clinoptilolite membranes made from dense mineral deposits by single gas H_2 and CO_2 permeation. Permeability values as a function of temperature and pressure were analyzed based on mass transport fundamentals of gas permeation through zeolite and non-zeolite pathways. Simple comparative parameters were introduced to characterize natural zeolite membranes. H_2 and CO_2 fluxes through the membranes were fitted with a model based on a combination of zeolitic, Knudsen and viscous transports so that the selective and non-selective flux fractions could be quantified.

Acknowledgments

“Whoever does not thank others, has not indeed thanked God.”

Mohammad (pbuh)

I would like to express my sincere gratitude to my supervisor, Prof. Steven Kuznicki, for his guidance, generous support and great encouragement during my studies. This dissertation would not have been possible without his kind attention and patience. I would also like to thank my examining committee, Dr. Greg Dechaine, Dr. Sushanta Mitra and Dr. Hongbo Zeng for their invaluable comments and suggestions.

I would like to sincerely acknowledge Dr. Adolfo Avila for his great guidance and hundreds of hours he devoted to my research. I am very grateful for his insights, advices and valuable discussions. It is also my pleasure to thank Dr. Tetyana Kuznicki, Mrs. An Weizhu and all the members of our research group for their valuable supports. I would like to thank Mrs. Albana Zeko for her assistance with manuscript development.

Finally, I would like to express my deepest gratitude to my family: My parents, Naser and Zohreh, and my brother, Mohammadreza. Although I lost my father six years ago, I would never forget him and his memories will stay with me forever. I am indebted to my mother for her patience, blessing and love. Therefore, this thesis is dedicated with love and respect to my parents.

Financial supports from Canada Research Chair (Tier I) in Molecular Sieve Nanomaterials (S.M.K.), Alberta Water Research Institute (S.M.K.) and Helmholtz Alberta Initiative (S.M.K.) are gratefully acknowledged.

Table of Contents

List of Tables

List of Figures

Nomenclature

Roman letters

A_i	*Non-zeolite area of membrane surface (m^2)*
A_t	*Total permeable area of membrane surface (m^2)*
A_z	*Zeolite area of membrane surface (m^2)*
b_i	*Langmuir adsorption constant of component i (Pa^{-1})*
$b_{i,0}$	*Langmuir adsorption constant of component i at (Pa^{-1})*
B_0	*permeability constant (m^2)*
d_k	*Kinetic diameter of gas molecule (m)*
d_p	*Pore diameter of the membrane (m)*
D_i	*Diffusivity of component i ($m^2\ s^{-1}$)*
$D_{i,0}$	*Diffusivity of component i at zero loading ($m^2\ s^{-1}$)*
$D_{i,kn}$	*Knudsen diffusivity of component i ($m^2\ s^{-1}$)*
D_F	*Fick's diffusivity ($m^2\ s^{-1}$)*
E_i^D	*Activation energy of component i ($J\ mol^{-1}$)*

f_i	*Fugacity of component I (Pa)*
K_i	*Henry's constant of component i (mol kg^{-1} Pa^{-1})*
$K_{i,0}$	*Henry's constant of component i at temperature T_0 (mol kg^{-1} Pa^{-1})*
Kn	*Knudsen number*
M_w	*Molecular weight (gr mol^{-1})*
$N_{i,k}$	*Knudsen flux (mol m^{-2} s^{-1})*
$N_{i,v}$	*Viscous flux (mol m^{-2} s^{-1})*
$N_{i,z}$	*Molar flux through zeolite pores (mol m^{-2} s^{-1})*
$N_{i,nz}$	*Molar flux through non-zeolite pores (mol m^{-2} s^{-1})*
$N_{i,t}$	*Total molar flux (mol m^{-2} s^{-1})*
P	*Pressure (Pa)*
P_i	*Partial pressure of component i (Pa)*
P_m	*Mean pressure (Pa)*
q	*Adsorption capacity (mol kg^{-1})*
q_s	*Saturation adsorption capacity (mol kg^{-1})*
r_i	*Defect size (m)*
$\langle r_i \rangle$	*Integral mean of defect radii distribution (m)*

$\langle r_i^2 \rangle$	*Integral mean of -distribution of squared defect radii (m^2)*
r_k	*Defect size larger than r_i (m)*
r_m	*Flow averaged defect size (m)*
R_g	*Ideal gas constant ($J\ K^{-1} mol^{-1}$)*
S^i	*Ideal selectivity*
S^{kn}	*Knudsen selectivity*
T	*Temperature (K)*
T_0	*Reference temperature (K)*
$T(\theta_i)$	*Thermodynamics correction factor*
u	*fluid diffusion velocity in the zeolite crystals ($m\ s^{-1}$)*
x	*Distance (m)*

Greek letters

α_v	*Coefficient defined by eq 17 (mol m^{-1} s^{-1} Pa^{-2})*
β_{kz}	*Coefficient defined by eq 18 (mol m^{-1} s^{-1} Pa)*
ΔH_i	*Enthalpy of adsorption of component i (J mol^{-1})*
ΔX	*Membrane thickness (m)*
θ	*Fractional loading*
λ	*Coefficient defined by eq 20 (mol $K^{0.5}$ m^{-1} s^{-1} pa^{-1})*
μ	*Viscosity (Pa s)*
μ_0	*Viscosity at reference temperature (Pa s)*
μ_i	*chemical potential of component I (J mol^{-1})*
Π_i	*Membrane permeance of component i (mol Pa^{-1} m^{-2} s^{-1})*
$\Pi_{i,z}$	*Zeolitic permeance of component i (mol Pa^{-1} m^{-2} s^{-1})*
ρ	*Density of zeolite (kg m^{-3})*
ω	*Coefficient defined by eq 21 (mol m^{-1} s^{-1})*

Chapter 1. Introduction

It is anticipated that global energy consumption is going to increase by 50% in the next twenty-five years[1]. Furthermore, current environmental problems have created a need for cleaner fuels. Hydrogen has been proposed as a clean fuel. Hydrogen is plentiful and can produce the largest amount of energy per unit of weight among different kinds of fuels[2]. Fuel cell technology can produce electrical energy from H_2 stream. Using hydrogen as a fuel can reduce greenhouse gas emissions as the only by-product of its combustion reaction is water. Moreover, hydrogen is currently being used in many petrochemical industries such as hydrodesulphurization, hydrocracking and is the main feed stock for the production of methanol, ammonia, alcohols, hydrochloric acid, syngas and many other chemicals[3,4]. It is also widely used in metallurgical, pharmaceutical and textile industries[5].

1.1- Hydrogen production

Unfortunately, the problem with hydrogen production is that it does not exist in a free molecule form[6]. Around 90% of today's hydrogen is produced from reforming of natural gas and coal and it is anticipated to be the main process for H_2 production in the future[3]. Around 8% of hydrogen production is through electrolysis of water[5]. Water electrolysis

produces hydrogen with a very high purity; however, it consumes a lot of electricity and does not seem to be applicable for large scale hydrogen production. The other method of producing hydrogen is coal gasification. The problem associated with this method is that the production process contains a lot of side reactions which reduce the efficiency of the process. Natural gas reforming efficiency for producing hydrogen is relatively higher than coal gasification method (70-80%)[7].

Using natural gas and coal for H_2 production involves two steps. The first step is natural gas steam reforming and coal gasification to produce syngas ($CO+H_2$). This step is performed at high temperature conditions (600-900 C) and pressures of 5-25 bars. The following equations describe these two high temperature processes:

$$\text{Steam reforming: } CH_4 + H_2O \Longrightarrow CO + 3H_2 \qquad (1\text{-}1)$$

$$\text{Coal Gasification: } C + H_2O \Longrightarrow CO + H_2 \qquad (1\text{-}2)$$

The second step is water gas shift reaction to produce more hydrogen by converting carbon monoxide to CO_2 and H_2:

$$CO + H_2O \Longrightarrow CO_2 + H_2 \qquad (1\text{-}3)$$

There are many side reactions aside from the main process. The output of coal gasification process usually contains 73.9% H_2, 17.7% CO_2, 6.9% CH_4 and 1.0% CO plus N_2, H_2O and Sulphur. Therefore, it is necessary to separate H_2 from other gases and impurities[3,5].

Another method of hydrogen production is dry reforming of natural gas[8]:

$$CH_4 + CO_2 \rightarrow 2CO + 2H_2 \quad (1\text{-}4)$$

There are other methods of hydrogen production but the common point between most of these methods is that hydrogen is produced in a mixture with other gases and impurities. After such reactions, hydrogen must be separated from methane, carbon dioxide and smaller amounts of other gases before it can be used as fuel[9].

1.2- Hydrogen separation

There are four major methods for hydrogen separation from mixtures: chemical and physical absorption, pressure swing adsorption, cryogenic distillation and membrane separation technology[4]. Absorption techniques have been used to remove CO_2 from H_2 after natural gas steam reforming unit. Potassium carbonate and amines were used as the scrubber. This method does not produce hydrogen with high purity[10] (higher than 95%).

Pressure swing adsorption (PSA) is one of the most common method for hydrogen separation from gas mixtures. The first PSA unit was introduced in 1960 by Skarstrom[11]. The main advantages of the PSA process is that it can produce very high-purity hydrogen (over 99%) and the adsorbent can be easily regenerated. However, its process design is

complicated and it is difficult to be used in a continuous separation process. Temperature swing adsorption (TSA) can also be used to separate hydrogen but it is too time consuming to slowly cool and heat the system during each cycle of the TSA[2].

Cryogenic distillation separates components based on their boiling temperatures. There are a number of disadvantages with using this method such as the need for an additional methane wash column to separate hydrogen from CO or CO_2. This method requires high energy while still not producing a high level purity product[2].

Among the methods mentioned PSA and cryogenic distillation are widely used to separate hydrogen from mixtures in industrial scale. However, these methods are not practical to produce hydrogen as fuel because in the end they cannot compete with petroleum fuels' prices[3].

The separation process is a vital step in chemical process industries. Hydrogen separation and purification's cost is responsible for a large part of the capital investment of a large scale chemical plant[12]. It is anticipated that 20% improvement in hydrogen separation in natural gas reforming process could result in substantial energy savings annually[4].

During the past decade, membrane technology was introduced as an alternative for conventional hydrogen separation methods. Membranes are basically physical barriers that are able to separate a mixture into its various components based on their size or shape. Moreover, it is a simple

process and the energy requirement is significantly lower compared to other separation methods because it does not involve any phase change step in the separation process[3]. In addition to this, membrane separation processes can be carried out in a space efficient continuous operation[2]. Membrane technology has a low investment cost and is easy to scale up. Based on these advantages, membrane-based processes have the potential to replace the conventional hydrogen separation techniques.

1.3- Scope of research

Current hydrogen separation membranes are made of palladium alloys or chemically and mechanically unstable organic polymer membranes[13]. Palladium membranes are costly, and can only be utilized at high temperatures[13]. Organic polymer membranes are thermally and mechanically unstable and cannot tolerate sulphur and hydrochloric acid. Zeolite membranes are great choices for hydrogen separation processes due to their high thermal, chemical and mechanical stability[6]. Zeolite molecular sieves have uniform pore sizes which could make them promising for this separation. Natural Zeolite membranes are capable of separating compounds by a combination of molecular sieving, selective adsorption, and differences in diffusion rates[14,15,16,17,18,19,20,21]. Synthetic molecular sieve membranes for hydrogen separation have also been studied intensively; however, their applications have been limited by high

production costs, lack of mechanical integrity (cracks or defects), and poor physical and chemical compatibility between the sieves and the supports on which they are grown[22,23]. While extensive research has been performed on the potential for hydrogen purification by synthetic molecular sieve membranes[24,25,26], little attention has been paid to the natural zeolite-based membranes and their potential applications for hydrogen purification.

Natural zeolite membranes, which have been compacted by time and nature, have recently been shown to demonstrate apparent molecular sieving of H_2 from H_2/CO_2 mixtures[27]. Such membranes are mechanically robust and with modification and development may enhance the utility of molecular sieve membranes in many large scale separation processes. Because of the prolonged time and pressure that some natural zeolite deposits have experienced, intercrystalline grain boundaries, the primary weakness of synthetic zeolite membranes, have been fused or eliminated; leaving materials with mechanical integrity unlike that of the synthetic analogs.

This work focuses on the characterization of disk-shaped natural clinoptilolite membranes by single H_2 and CO_2 permeation. H_2 and CO_2 fluxes through the membranes were obtained both experimentally and mathematically (by fitting with a model based on the combination of zeolitic, Knudsen and viscous transports). Comparative parameters were

introduced to characterize the membranes based on the relative average defect size, the cross sectional area of the non-zeolite pores and the diffusion coefficients. This is necessary for the quantification of the selective flux (zeolite and Knudsen fluxes) and non-selective flux fraction (viscous flux) for each membrane analyzed. This characterization method is useful to understand the membrane behavior and to predict its permeation and selectivity at different operational conditions. The simulation of membrane permeance assists in the analysis of experimental observation of different membranes and set up a basis to study the effect of membrane modification on the membrane's performance.

Chapter 2. Background

2.1. Membranes for hydrogen separation

As discussed in the introduction, membrane technology offers many advantages compared to conventional gas separation methods. One of its potential applications could be in the CO_2 capture related area such as post-combustion capture where CO_2 should be removed from a mixture of N_2, H_2O and O_2.[28] Presently, chemisorption with amines is the technology used by industry for this separation. CO_2/N_2 selective membranes have already been introduced for post-combustion CO_2 capture in power plant[29]. Membranes are also able to separate azeotropes and components with close boiling points which is problematic in conventional separation methods such as distillation[30]. Membrane technology can also be combined with water gas shift reactors (WGS) to increase their efficiency by separating hydrogen from the product. As a result, WGS reaction will shift into the product side and yield more hydrogen[31].

The first large scale gas separation unit was installed by Permea company for the separation of hydrogen from ammonia reactor purge gas using polysulfone hollow-fiber polymer membranes. Later, Cynara, Separex and GMS Company started to use cellulose acetate membranes for the separation of CO_2 from natural gas while Generon Company used TPX membranes for air separation purposes[32]. The four commercially important gas separations are H_2/CO_2, H_2/CH_4, CO_2/CH_4

and O_2/N_2 separations. In this chapter we will focus on the membranes used for H_2 separation. There are five types of membranes described in literature for H_2 separation: polymer, metal, silica, zeolite and carbon membranes[6]. The last four are inorganic membranes while polymer ones are organic membranes. Inorganic membranes are divided into two groups: Dense (metal membranes) and porous (carbon, silica and zeolite membranes).

US department of Energy has suggested the following five targets for an efficient H_2 membrane separation process: (1) higher H_2 permeance; (2) lower material cost; (3) enhanced durability; (4) lower power requirement; (5) lower membrane production cost[5]. Two main desired factors in membrane separation processes are high selectivity and high flux or permeance through the membrane. Membrane flux is the total mass or moles of molecules passing through the membrane per unit time per unit area. Total permeance is the total flux per unit partial pressure difference between feed and permeate side of the membrane. Membrane's selectivity represents the separation ability of the membrane.

Among the inorganic membranes, silica membranes are not stable at high temperature and humid conditions. Carbon-based membranes are made by carbonization of organic polymers[6] and are fragile and expensive. They are not stable in the presence of H_2S and their hydrogen permeance is low[2]. Organic polymer membranes and dense metallic membranes are popular amongst researchers for H_2 separation. Therefore, in the following two sections we will focus on organic polymer and metal membranes for H_2 separation.

2.1.1. Polymer membranes for hydrogen separation

Organic polymer membranes are extensively being used for hydrogen separation in industrial scale. Cellulose acetate, polyimide and polysulfone membranes are the first generation of commercial membranes for hydrogen separation[33]. Polymer membranes have low manufacturing cost for industrial application and can tolerate high pressure drop conditions[2]. Furthermore, hollow fiber polymer membranes with high surface area-to-volume ratio can be easily made out of these materials[6].

Polymer membranes separate H_2/CO_2 based on solution-diffusion mechanism. A component should first dissolve into the membrane and then diffuse through the membrane. There are two groups of polymer membranes: glassy and rubbery. Generally, glassy polymer membranes have high selectivity and low permeance. On the other side, rubbery polymer membranes have low selectivity and high permeance. Glassy polymer membranes are able to separate hydrogen due to its smaller size than other gases. Rubbery polymer membranes are able to separate CO_2 based on its higher solubility in the polymer than H_2. However, polymer membranes are not mechanically stable and cannot tolerate H_2S and hydrochloric acid. In addition to this, these membranes can only be operated at low temperature conditions[2]. High pressure conditions may also result in plasticization in these

membranes in the presence of CO_2.[34] Due to organic polymer membranes' limitations, many efforts have been directed toward using inorganic membranes.

2.1.2. Dense metallic membranes for hydrogen separation

Dense metallic membranes such as palladium (Pd) membrane have been widely used for Hydrogen separation. These membranes adsorb H_2 and dissociate it into two H atoms. These atoms will be transported through the membrane and will associate together on the permeate side[6]. These membranes offer very high selectivity and reasonable permeance for H_2 due to the intrinsic transport mechanism and the possibility of achieving thin metallic films[3], Many researchers are using Pd membranes for H_2 separation. Although it is possible to use other metals such as Nb, Ta and V, they form metal oxide layers on the surface of the membrane which will hinder hydrogen permeation through the membrane. Nevertheless, these membranes have higher permeability compared to palladium membranes[2].

Metallic membranes have many limitations. These membranes require high temperature conditions to attain reasonable permeance[5]. Palladium membranes are reported to be fragile and sensitive to sulphur and carbonaceous conditions. In addition CO can get adsorbed to the surface inhibiting H_2 diffusion[3].

Inorganic zeolite membranes have attracted many researchers' attention due to their unique properties. Zeolite membranes are great choices for gas separation

processes due to their high thermal, chemical and mechanical stability[6]. In the following sections an overview on zeolite materials and their applications in the membrane process technology is given.

2.2. Zeolite molecular sieves

2.2.1. Zeolite's structure and properties

The term zeolite was used by Swedish scientist, Axel Cronstedt in 1756 for the first time[35]. It consists of two Greek words: “zein” which means “boil” and “Lithos” meaning “stone”. When Cronstedt heated the zeolite stone, the adsorbed water in the zeolites boiled making it appear as if the mineral is boiling. Zeolites have crystalline frameworks with uniform pores and high surface area up to hundreds of square meter per gram of zeolite. Their structure is made up of TO_4 tetrahedral units (T can be Si, Al, B, Ge, etc.)[5]. TO_4 tetrahedrals share an oxygen atom with another tetrahedral and form chains. In other words, each T atom is connected to four oxygen atoms and each oxygen atom is linked to two T atoms to form chains. The chains connect to each other to form rings or secondary building units. These connections are extended 3-dimensionally to form a framework structure. More than 190 zeolite framework structures are known. The international zeolite association have assigned a three letter code for each framework topology such as LTA, FAU and MOR. Each framework covers many zeolites with different types of composition[36].

In general the zeolite framework is made up of tetrahedral units of SiO_4 and AlO_4^-. SiO_4 molecules are neutral but AlO_4^- has a net negative charge. Thus, the framework is negatively charged and it has to be balanced by an external cation. It can be balanced with typical cations such as Na^+, Li^+ or Ca^{2+}. These cations are located in the zeolite channels and not inside the zeolite framework. Therefore, they are mobile and can be easily exchanged. Ion exchange is basically exchanging the ions of the insoluble material with the ions in the solution. The ability of zeolites to perform ion-exchange has made them popular amongst researchers for their potential applications. A zeolite containing sodium or potassium cations can be used for water softening applications by exchanging Na or K with Calcium, magnesium or ammonium ions in water or waste streams.

The most important characteristic of zeolites is that they contain small channels and pores that are great for separation of small molecules. With regard to their crystalline structure, zeolites have narrow pore size distribution. Each secondary building unit contain open rings. These rings are set together in a row to make channels through the zeolite structure. The pore aperture in zeolite materials is around 0.3- 1.0 nm and is comparative to the kinetic diameter of the gas molecules. This makes zeolites potential materials for selective gas separation based on differences in kinetic diameter of molecules. Kinetic diameter is the smallest limiting cross sectional dimension of the molecule. Table 2.1 summarizes this parameter for some of the gases.

Table 2.1. Kinetic diameter of gases[35,37]

Gas	Kinetic Diameter (nm)
Helium (He)	0.26
Hydrogen (H_2)	0.28
Carbon dioxide (CO_2)	0.33
Oxygen (O_2)	0.34
Nitrogen (N_2)	0.36
Methane (CH_4)	0.38
n-butane (n-C_4H_{10})	0.43
Iso-butane (i-C_4H_{10})	0.50

The pore size in zeolites depends on the number of T atoms in each ring in the structure. Based on this, there are five main groups of zeolite: 6-membered rings, 8-membered rings, 10 membered rings, 12 membered rings zeolites and 16-membered rings[5]. Table 2.2 lists the average pore aperture for each group. Different cations can also change the pore size of the zeolite molecular sieves. For instance, Na exchanged zeolite A has a pore opening of about 4 angstrom. However, if sodium is exchanged with potassium that is a bigger cation than Na, pore opening will decrease to 3 angstrom. This behaviour can be advantageous in

small molecule gas separation[37]. Some studies suggest 0.3-0.4 nm as the minimum appropriate pore size of the membrane for H_2/CO_2 separation[38,39,40].

Table 2.2. Average pore aperture for zeolite membrane[37]

Rings	Pore aperture (nm)	Example	Separation Application
6-membered ring	0.26	Sodalite	H_2O/H_2
8-membered ring	0.30-0.45	Zeolite A	Straight chain Hydrocarbon
10-membered ring	0.45-0.60	ZSM-5	Xylenes
12-membered ring	0.6-0.90	Zeolite X, Y	Long chain hydrocarbons
16-membered ring	1.00-1.20	VPI-5	Small biological molecules

Si/Al ratio is another key parameter of zeolite materials. Zeolites with higher Si/Al ratio have higher stability. Both catalytic activity and ion-exchange capacity increases with a decrease in Si/Al ratio. Lower Si/Al ratio increases hydrophobicity of the zeolite. Si/Al ratio may have minor effects on the pore size of the zeolite as well. Aluminum-Oxygen bond is longer compared to Silica-

Oxygen bond. Therefore, lower Si/Al ratio or higher aluminum content may slightly affect the pore size of the zeolite and make it larger[41].

Water present in the zeolite structure can be removed by calcination. As a result, the channels in zeolites' framework are ready for adsorbing other molecules. Adsorption behaviour of the zeolites depends on many factors such as polarity of the adsorbate, operating temperature and pressure, zeolite framework and composition.

2.2.2. Zeolite membranes' applications

As discussed in section 2.1.1, organic polymer membranes are widely used for industrial gas separation applications. However, due to their shortcomings, many efforts have been directed toward using inorganic membranes and zeolite membranes in particular. Zeolite membranes offer numerous advantages over other types of inorganic membranes[42]. They have higher thermal and chemical stability compared to other membranes and are able to tolerate high pressure drop[43]. As mentioned in the previous chapter, zeolite membranes have uniform pore size of 0.3-1 nm which is comparative to diameters of many gas molecules. Therefore, these membranes can perform molecular sieving or size exclusion in gas separation processes. Molecular sieving occurs when one of the molecules in the mixture is bigger than the pore size of the zeolite and it is being screened off from the mixture by the membrane. New applications such as catalytic membrane

reactors have increased the attention toward zeolite membranes because of their numerous advantages such as temperature stability and solvent resistance[43].

Synthetic zeolite membranes consist of a thin zeolite layer on a support, often made of ceramics or stainless steel. ZSM-5 (Zeolite Second mobile five) or MFI zeolite membranes are widely being studied for hydrogen separation such as the separation of H_2 form hydrocarbons[44]. SAPO-34 membranes were also reported for CO_2/CH_4 separation with high selectivity[45]. Other membranes such as zeolite Y are also used for CO_2/N_2 separation[46]. Zeolite membranes are also useful in catalytic industries as they separate one of the products and as a result, shifting the reaction equilibrium to obtain higher conversions[47]. MFI zeolite membranes have been reported in catalytic de-hydrogenation of i-butane by separating H_2 under equilibrium conditions[23].

In addition to gas separation's applications, zeolite membranes have found uses in many other areas. LTA zeolite membranes can potentially separate water from ethanol or other organic solutions and offers high selectivity values[23]. FAU membranes were reported for separation of alcohols[48]. The biggest application of zeolites in the world is Zeolite A used in detergent industries for water softening[49].

Another use for zeolite membrane separation techniques is replacing traditional separation methods of xylene isomers as they consume less energy. MFI membrane's pore size is comparable to benzene molecules. Thus, this zeolite may be useful in separation of xylene isomers. P-xylene can pass the zeolite pores but

o-xylene and m-xylene are screened out. Gu et al. have reported separation of p-xylene by MFI membranes[50].

Despite zeolite membranes many advantages over organic membranes the only commercialized application is water separation from ethanol using zeolite NaA membrane, in use mainly by Mitsui Engineering and Shipbuilding Co[51].

Synthetic zeolite membranes have found limited applications in industry because of the difficulty in reproducing the desired thin zeolite layer in an industrial scale[52]. One of the issues for synthetic zeolite membranes such as MFI and DDR is that the thermal expansion coefficient while positive at near ambient temperature is negative at higher temperatures. This behaviour is different from the expansion coefficients of typical metal or ceramic supports that increase with temperature and therefore can cause problems in attaching the zeolite layer to the support[43]. Pina et al.[51] have mentioned the cost and difficulties in reproducing and preparing these materials such as non-uniform crystal grown, as the main reasons for slow improvement in industrializing zeolite membranes. The main cost of producing these membranes is due to expensive ceramic supports. However, the authors have reported many new small-scale applications for zeolite layers[51]. The other difficulty stated by Caro et al. is anisotropy of pores in zeolite membranes which will result in non-uniform mass transport through the membrane[43]. Zeolite's defects or pin holes are one of the major concerns in zeolite membranes. These defects can be in the form of impurities or crystal intergrowth defects. These non-zeolitic pores can significantly reduce membrane's selectivity. To

overcome these problems, many researchers have started working on mixed matrix membranes to incorporate advantages of zeolite membranes such as hydrothermal stability with polymer membranes' advantages like simple processing procedure[23].

Natural zeolite membranes can provide many advantages compared to synthetic zeolite membranes. They are inexpensive and uniformly porous and their preparation process is not complicated. An et al.[27] have recently shown apparent molecular sieving of H_2 from H_2/ CO_2 mixtures by natural zeolite membranes.

2.2.3. Natural zeolite molecular sieves

Natural zeolites molecular sieves are natural mineral deposits that have been metamorphosed by time and pressure over millions of years until they form solid masses[27]. They can be formed from volcanic ashes, clay and quartz and are usually found in volcanic rocks deposits all around the world. These materials are inexpensive and plentiful around the world. Natural zeolites have a high internal surface area which can be advantageous in catalysis applications. Furthermore, they can be used as acid cracking catalysts if the alkaline or the alkaline-earth cation in the structure of the zeolite is replaced with H^+.[53] Natural zeolites can be used as membranes for gas separation purposes because of their high chemical, thermal and mechanical stability. they can offer great molecular sieving for gas

molecule separation. Table 2.3 summarizes advantages and disadvantage of different methods of hydrogen separation.

Table 2.3. Advantages and disadvantages of different methods of hydrogen separation

Method	**Cost**	**Energy/Water Consumption**	**Stability**	**Scale up**
Cryogenic Distillation	✗	✗	✓	✓
PSA/TSA	✗	✗	✗	✓
Palladium Membranes	✗	✓	✗	✗
Polymer Membranes	✗	✓	✗	✓
Synthetic Molecular Sieves Membranes	✗	✓	✗	✗
Natural Zeolite MS Membranes	✓	✓	✓	?

Among natural zeolites clinoptilolite, chabazite, mordenite, erionite, ferrierite and phillipsite are considered to have the most potential in industrial gas separation applications[54]. Clinoptilolite is the most common type of natural zeolites. Clinoptilolite is derived from the Greek words “klino”, “ptylon” and “lithos” meaning “oblique feather stone”. Clinoptilolite has a two-dimensional (2D) micropore/channel structure. The framework of clinoptilolite contains three sets of intersecting channels (A, B, C). The channels A and B are parallel to the c-axis and channels C are parallel to the a-axis. Channels A are formed by strongly compressed ten-membered rings (aperture 4.4 x 7.6 Å), and the B channels are confined by eight-membered rings (aperture 4.7 x 4.1 Å). The C channels are also formed by eight-membered rings (aperture 5.5 x 4.0 Å)[55,35]. Figure 2.1 shows clinoptilolite framework structure. Clinoptilolite chemical formula can be expressed as $(Na_2,K_3,Ca)\,[Al_6\,Si_{30}\,O_{72}]\,24(H_2O)$ [56].

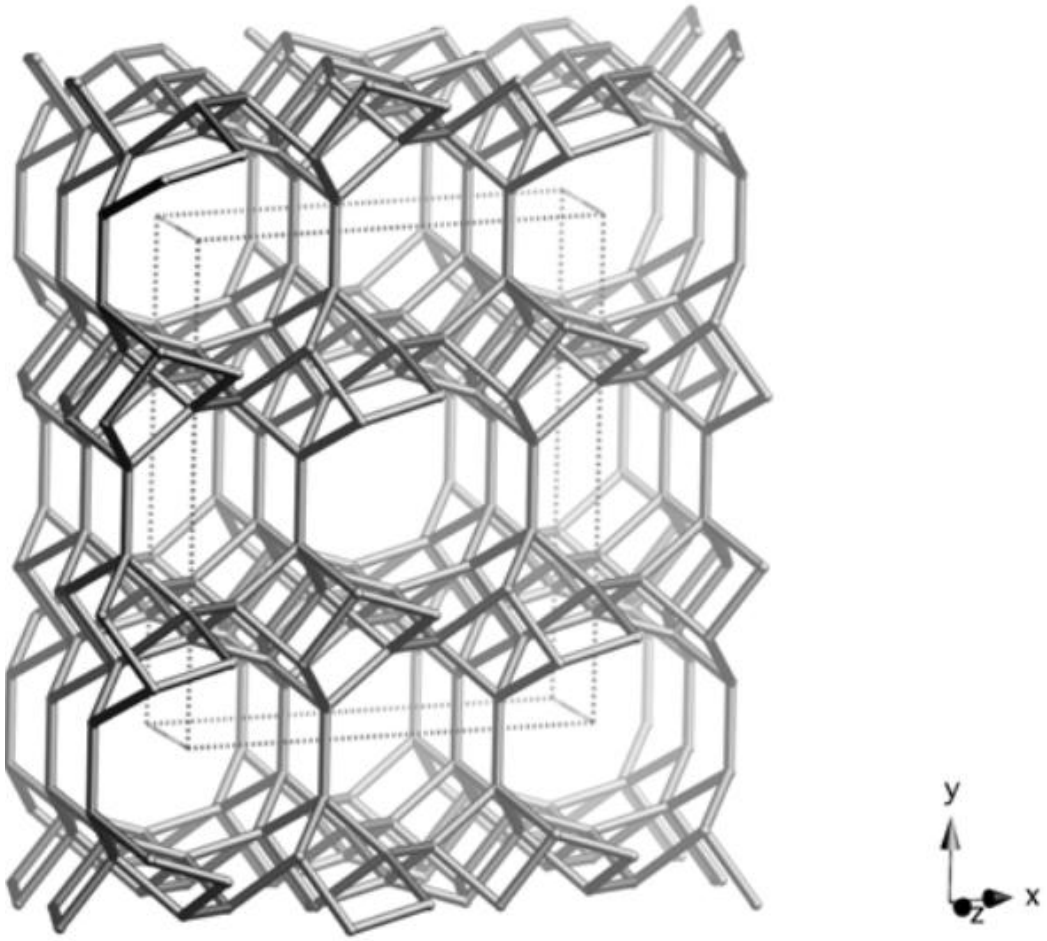

Figure 2.1. Clinoptilolite framework structure[36]

Clinoptilolite has found uses in separation industries. Aguilar-Armenta et al. have reported separation of C_2H_4/C_2H_6 mixtures with cation exchanged clinoptilolite[57]. The same authors have also used clinoptilolite to separate N_2 from O_2, N_2 from CH_4 and CO_2 from CH_4 mixtures[58]. Clinoptilolite is shown to remove Pb^{2+}, Cu^{2+}, Cr^{2+} and Fe^{2+} from aqueous solutions due to its ion-exchange capability[59],[60].

In this study, clinoptilolite minerals from the deposit at Castle Mountain (New South Wales, Australia) and from the deposit in Mount Kobau (British Columbia, Canada) have been used. These materials are unusual and have been compressed by their environments to the point where they have essentially no macroporosity. With bulk densities often approaching 2.5 g/cm^3, approximating the value expected for a single clinoptilolite crystal, these materials may in some ways be regarded as a solid crystalline zeolite block. Natural zeolite based membranes made from these deposits were characterized in this study. Figure 2.2 shows a clinoptilolite sample used is this study.

Figure 2.2. Sample clinoptilolite mineral, BC, Canada

Chapter 3. Experimental*

This research is focused on characterization of natural zeolite membranes by modeling single gas permeance through the membranes. Conducting experimental tests was not part of this research. The necessary experimental work was conducted by other team members in Dr. Kuznicki's group. In order to provide a background to aid in the understanding of the simulation data a brief overview of the experimental part is discussed in this chapter.

3.1 Membrane preparation

The natural zeolite rocks used in this study were from different deposits from all around the world. Different kinds of zeolites such as clinoptilolite and sodalite from different deposits from Canada, Australia and other parts of world were studied. Two membranes from two different batches of the deposit located in Mount Kobau, British Columbia, Canada are compared in chapter 5 of this thesis. Mount Kobau is located approximately at N 49^{o} 14' 49", W 119^{o} 43' 59", and elevation of 1317m. Natural mineral rocks were sectioned into thin disc shape membranes with thicknesses of 2.2 mm and 2.1 mm each using a diamond saw. These membranes were polished with a diamond polishing lap (180 mesh, Fac-

* A version of this chapter has been submitted for publication to the journal of Industrial & Engineering Chemistry Research (ACS Publications).

Ette Manufacturing Inc.) and then washed in an ultrasonic bath of deionized water for 30 min. Before each permeation test, the clean discs were dried in a temperature programmable oven using a two-step temperature program at a ramp rate of 0.1^{o}C/min from room temperature to 120^{o}C and 2^{o}C/min from 120^{o}C to 300^{o}C and finally held at 300^{o}C for 2 hr[27]**.** XRD analyses were carried out on these materials using a Rigaku Geigerflex Model 2173 diffractometer with a Co tube and a graphite monochromator.

A JEOL 6301F field emission scanning electron microscope supplemented with energy dispersive x-ray spectroscopy (EDX) was used to examine the surface morphology of the membranes. The analysis results are summarized in Table 3.1. More discussion is provided in section 5.1.4.

Table 3.1. Chemical composition (normalized wt.%) of the membrane sample, determined by energy dispersive X-ray analysis

Sample	**M1**	**M2**
Fe	3.25	8.24
Ca	6.02	7.04
Mg	0.78	1.76
Al	8.83	11.47
Si	47.95	45.55
K	2.88	2.88
Na	0.68	1.96
Cl	0	0
Ti	0.32	0.64
O	29.29	20.64

3.2 Adsorption isotherms

CO_2 isotherms for the mineral zeolite membranes were obtained by a volumetric method on an Autosorb-1MP volumetric system (Quantachrome Instruments, Boynton Beach, FL) at temperatures of 298, 323 and 343 K and at pressures up to 100 kPa. The samples were activated at 573 K for 12 h under vacuum of greater than 10^{-4} Torr before adsorption tests. An example of CO_2 isotherm at 298 K on these materials is shown in figure 3.1.

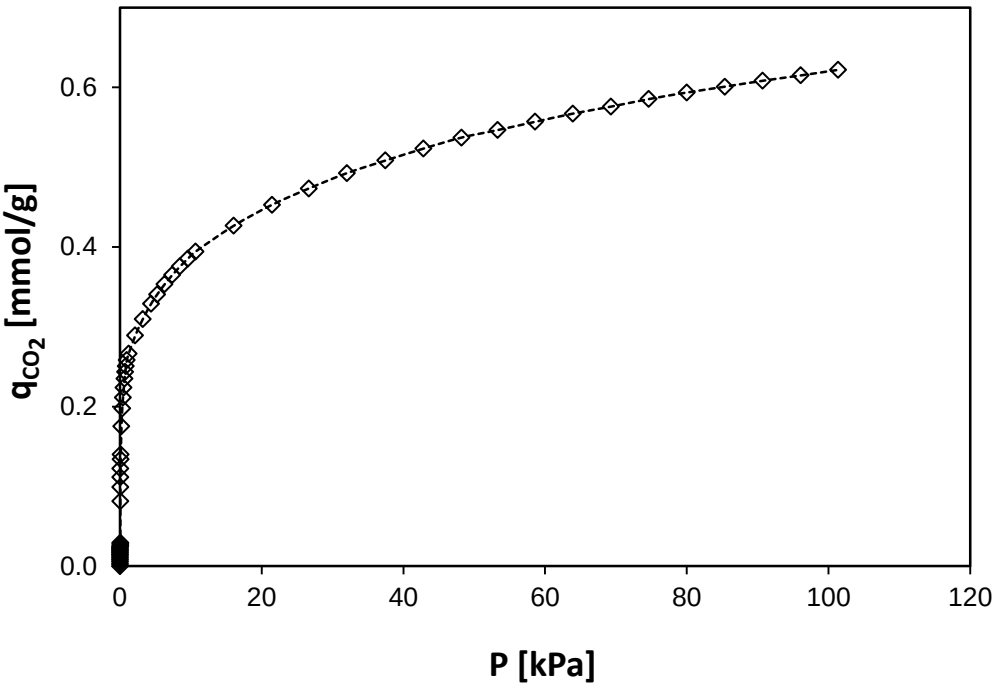

Figure 3.1. CO_2 isotherms of a membrane at 298 K.

3.3 Gas permeation measurement

Gas permeation through the membranes was measured in a lab-made membrane testing system. The configuration of the membrane cell is schematically shown in Figure 3.2.

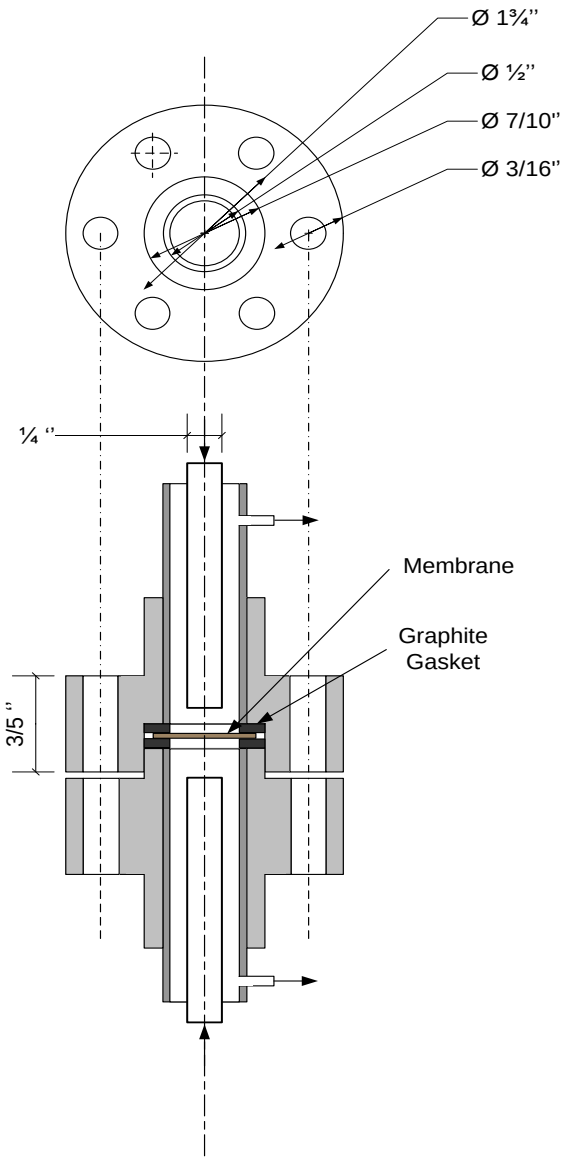

Figure 3.2. Configuration of a membrane cell

The membranes were mounted into a stainless steel cell and sealed with graphite gaskets. The feed and permeate sides each had a stainless steel tube-shell configuration with an inlet gas flowing through the ¼" inside tube and an outlet gas flowing through the shell between the ¼" inside tube and ½" outside tube. Argon (obtained from Praxair Canada, Inc) was used as a sweep gas for the permeate side. The feed side pressure was controlled by a back pressure regulator and the permeate side was kept at ambient pressure. The flow rate of the feed side and the flow rate of the sweep gas (Ar) were kept at 100 mL/min (STP) and 200 mL/min (STP) respectively throughout the measurements. The membrane cell was placed into a tube furnace with a multipoint programmed temperature controller.

Single gas permeation of H_2 and CO_2 (obtained from Praxair Canada, Inc) was measured at temperatures ranging from 298 K to 573 K and feed pressures from 101.35 kPa to 202.70 kPa. For the gas composition analysis, an on-line gas chromatograph (GC; Shimadzu GC-14B) with a HayeSep Q packed column and a thermal conductivity detector was used. Experimental permeation data were compared with model prediction in order to obtain model parameters based on the fitting process.

Chapter 4. Modeling*

4.1- Introduction to gas transport through zeolite membranes

The modeling and simulation of gas transport through zeolite membranes is a useful tool to understand the membrane behavior and to predict its permeation and selectivity at different operational conditions. Simulation of membrane permeance is useful for the analysis of experimental observation of different membranes and for studying the effect of membrane modification on membrane performance.

Gas transport through a molecular sieve membrane is due to contributions from both zeolite and non-zeolite fluxes. However, in many studies, membrane structure is assumed to be homogeneous and defect-free[61]. Non-zeolitic flux through membrane defects can play an important role in the overall transport mechanism through the membrane. Permeation mechanism through a membrane depends on many parameters such as interactions between gas molecules and membrane's pore wall and experimental operational conditions such as temperature and pressure[3]**.** Pore diameter, pore wall structure, interconnection structure of channels and molecule-molecule interactions also affect mass transport mechanisms across the membrane[62]**.** Different transport mechanisms are able to contribute to the total flux through a zeolite membrane such as surface

* A version of this chapter has been submitted for publication to the journal of Industrial & Engineering Chemistry Research (ACS Publications).

diffusion (also known as intracrystalline, microporous, configurational or activated diffusion) through zeolite crystals and Knudsen and viscous mechanisms through non-zeolite sites. The molecules diffusing through the zeolitic channel are considered to be unable to escape from the force field of the pore walls, i.e., configurational diffusion, when the $\frac{d_k}{d_p}$ (d_k: kinetic diameter; d_p: pore diameter) ratio is high. Configurational diffusion mechanisms can occur from values of $\frac{d_k}{d_p}$ of about 0.6 in some cases depending on the configuration of the molecule and temperature[88].

Hanebuth et al. have assumed only Knudsen diffusion for H_2 through silicate-1 membranes[61]. They have modeled the flux through the zeolite based on a combination of Knudsen, activated and surface diffusion. They have also used dusty gas model to simulate the flow mechanism through stainless steel support of their MFI membrane. Markovic et al. reported gas separation through porous glass membranes with relatively narrow pore size[63,64]. In this study they have neglected viscous flow and considered activated diffusion through 1.4 nm pores. Molecular sieving happens when pore size of the membrane is between the kinetic diameters of the two gas molecules. In general, viscous mechanism dominates when the membrane contains defects or relatively large pores and the separation process is performed at high pressure drop conditions[3]. However, the estimation of the Knudsen number (Kn), which is the ratio of the mean free path to the pore radius ($Kn = \frac{\lambda}{r}$), indicates whether Knudsen diffusion or viscous flow dominates. For Kn > 10, transport is predominantly driven by Knudsen diffusion, and for Kn <

0.01, viscous flow dominates[65]. For Kn numbers between 0.01 and 10, both Knudsen diffusion and viscous flows contribute.

In addition to the testing difficulties associated with experiments, multicomponent transport modeling is complicated further as one should take into account different kinds of interactions such as competitive adsorption and pore blocking[61,66]. This will result in a complex set of coupled equations for multicomponent systems. In this study we will focus on single gas permeation modeling.

Single gas permeance is modeled based on a combined contribution from intracrystalline diffusion through zeolite cavities and Knudsen and viscous flow through non-zeolite pores. Potential transport pathways are depicted in Figure 4.1. Condensation permeation mechanism is ignored in this study because for light gases such as CO_2 and H_2, vapour pressure decrease in the pores is not significant enough to cause condensation in pores. Here we consider both the zeolitic and non-zeolitic fluxes through the membranes, assuming that these two pathways are not in a series. In other words, they are not passing through the same shared pathways. An overview on the theory of mass transport through zeolite and non-zeolite pores is discussed in the following sections 4.2 and 4.3.

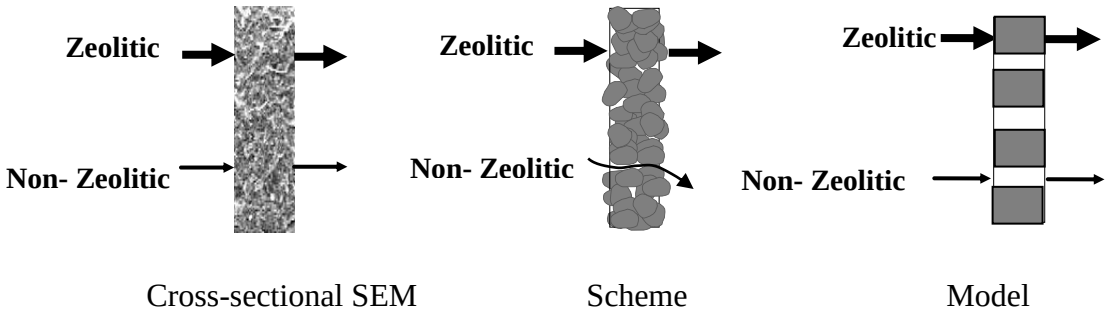

Figure 4.1. Outline of the gas transport pathways through the membrane.

4.2- Flow through zeolite pores

Gas transport through zeolite crystals is often referred to as surface diffusion, intracrystalline flux or zeolitic diffusion. Macroscopic and molecular dynamics are the two methods used to describe diffusion mechanism. Based on our experimental data (global permeance data) macroscopic model is the best choice to describe the diffusion though zeolite crystals. Molecular dynamics method is becoming important for estimating diffusion and adsorption parameters to be included in the macroscopic model (multi-scale model). In this study we have used macroscopic models to describe mass transfer through the zeolite membranes. The Maxwell-Stefan equation has been extensively used to describe

mass transport through zeolite crystals and it is considered as the best approach to quantify intracrystalline flux through zeolite membranes. Intracrystalline mass transfer through zeolites occurs through a combination of diffusion and adsorption mechanisms. The model used should take both of these mechanisms into account. Maxwell-Stefan formulation considers both the effect of adsorption and diffusion[67].

Five steps have been introduced to describe the transport mechanism of a gas molecule through a zeolite membrane: (1) Adsorption of the gas molecule on the external surface of the zeolite crystal; (2) Diffusion from the external surface into the zeolite crystal; (3) Diffusion through the zeolite channel; (4) Diffusion to the external surface of the zeolite crystal; (5) Desorption from the external surface of the zeolite to the bulk gas phase[5].

In theory the relative forces between the zeolite material and the diffusing species are assumed to be due to the driving force between them, the chemical potential gradient. This driving force is defined as:

$$-\nabla_{T,p}\mu_i = -\frac{R_g T}{D_i} u \tag{4-1}$$

where the parameter u is the fluid diffusion velocity in the zeolite crystals and D_i is the Maxwell-Stefan diffusivity of component i. The flux through the membrane is defined as:

$$N_{i,z} = -\rho q u\,, \tag{4-2}$$

where ρ is the zeolite density in $\frac{kg}{m^3}$ and q is the loading with the unit of mol per kilogram. If we place equation (4-2) into equation (4-1), the following definition for the flux through membrane can be obtained:

$$N_{i,z} = -\rho q_s D_i \frac{\theta_i}{R_g T} \nabla_{T,p} \mu_i \tag{4-3}$$

where $\theta_i = \frac{q}{q_s}$ is the fractional loading of component i. q_s is the saturation adsorption capacity of component i. Chemical potential can be defined as follows:

$$\mu_i = {\mu_i}^0 + R_g T ln(f_i)\,, \tag{4-4}$$

where f_i is fugacity of component i and ${\mu_i}^0$ is the chemical potential at reference temperature. At low pressure conditions, we can use partial pressure of the component in place of the fugacity. Therefore, we can rewrite the $\frac{1}{R_g T} \nabla_{T,p} \mu_i$ term as follows:

$$\frac{1}{RT} \nabla_{T,p} \mu_i = \frac{1}{\theta_i} \mathrm{T}(\theta_i)\, \nabla \theta_i \tag{4-5}$$

$$\text{Where } \mathrm{T}(\theta_i) = \theta_i \frac{\partial \ln f_i}{\partial \theta_i} = \frac{\partial \ln f_i}{\partial\, ln\theta_i} = \frac{\partial \ln p_i}{\partial\, ln\theta_i} = \frac{\partial \ln p_i}{\partial\, lnq_i} \tag{4-6}$$

$\mathrm{T}(\theta_i)$ is the thermodynamics correction factor. Thus, total flux can be described as:

$$N_{i,z} = -\rho q_s D_i\ \mathrm{T}(\theta_i)\, \nabla \theta_i = -\rho D_i\, \mathrm{T}(\theta_i)\, \nabla q_i \tag{4-7}$$

The famous Fick's equation for zeolites is:

$$N_{i,z} = -\rho q_s D_f \nabla\theta_i = -\rho D_f \nabla q_i \ , \tag{4-8}$$

where D_f is the Fick's diffusivity and the relationship between Fick's diffusivity and Maxwell-Stefan diffusivity is described as:

$$D_f = D_i \ \mathrm{T}\,(\theta_i) \tag{4-9}$$

Krishna et al.[67] have shown that Fick diffusivity changes with loading. However, Maxwell-Stefan diffusivity is constant with loading in many types of zeolites. This can be useful in predicting the component diffusivity at different loading based on its value at zero-loading.

Diffusivity has an Arrhenius type dependency with temperature:

$$D_i = D_{i,0} \exp\left[\left(\frac{E_i^D}{R_g}\right)\left(\frac{1}{T_0} - \frac{1}{T}\right)\right] \ , \tag{4-10}$$

where $D_{i,0}$ is the diffusivity of component i at the reference temperature (T_0= 298 K) and E_i^D is the activation energy for diffusion. Diffusivity can also be considered to be loading dependent based on the following equation:

$$D_i \ = D_{i,0}\,(1 - \theta_i) \ , \tag{4-11}$$

where D_{i,θ_0} is diffusivity of component i at zero loading. Diffusivity dependency on loading can also be described by Reed and Ehrlich model[68]. However, we

limited our model description to a constant diffusivity approach. This model was selected to assist us in the screening strategy for these membranes.

A one dimensional flux across the membrane was assumed. Thus, flux of one component can be expressed as:

$$N_{i,z} = -\rho q_s D_i \mathrm{T}(\theta_i) \frac{d\theta_i}{dx} \tag{4-12}$$

The loading inside the zeolite (θ_i) is related to the partial pressure of component *i* by means of an adsorption isotherm model. In this study we selected a Langmuir model because of its simplicity and it was able to describe well H_2 and CO_2 isotherms at moderate pressures. Langmuir model describes the pressure dependency of loading as below:

$$\theta_i = \frac{b_i P_i}{1+b_i P_i} \tag{4-13}$$

where b_i is the Langmuir adsorption constant of component i. Therefore, Thermodynamic correction factor $\mathrm{T}(\theta_i)$ can be calculated as the following:

$$\mathrm{T}(\theta_i) = \frac{\partial \ln p_i}{\partial \ ln\theta_i} = \frac{1}{1-\theta_i} \tag{4-14}$$

The parameter b_i in Langmuir model is dependent on temperature according to the Van't Hoff equation:

$$b_i = b_{i,0} \exp\left[\left(\frac{\Delta H_i}{R_g}\right)\left(\frac{1}{T_0} - \frac{1}{T}\right)\right] , \tag{4-15}$$

where $b_{i,0}$ is the Langmuir adsorption constant at the reference temperature (T_0= 298 K). b_i is decreasing with temperature since adsorption process is exothermic and ΔH_i is negative. ΔH_i can be calculated based on Van't Hoff equation. Considering equation (4-14) we can simplify equation (4-12) to:

$$N_{i,z} = -\rho q_s D_i \frac{1}{1-\theta_i} \frac{\partial \theta_i}{\partial x} \tag{4-16}$$

4.2.1- Model analysis

To calculate the steady state zeolite permeance through membrane there are two possible methods. Equation (4-16) can be solved analytically or numerically. Both methods were compared. The numerical analysis was done using MATLAB. "pdepe" command was used to solve the resulting partial differential equation in the numerical method. The steady-state values were within 2-6% for both methods. The analytical solution was obtained by integrating equation (4-16) over x , gives the zeolitic flux can be expressed as:

$$N_{i,z} = -\frac{\rho q_s D_i}{\Delta X}\int_{\theta_{i,feed}}^{\theta_{i,permeate}} \frac{1}{1-\theta_i}\,\partial\theta_i$$

$$= -\frac{\rho q_s D_i}{\Delta X}\ln\left(\frac{1-\theta_{i,feed}}{1-\theta_{i,permeate}}\right)$$

$$= -\frac{\rho q_s D_i}{\Delta X}\ln\left(\frac{1-\frac{b_i P_{feed}}{1+b_i P_{feed}}}{1-\frac{b_i P_{permeate}}{1+b_i P_{permeate}}}\right)$$

$$= -\frac{\rho q_s D_i}{\Delta X}\ln\left(\frac{1+b_i P_{permeate}}{1+b_i P_{feed}}\right) \qquad (4-17)$$

The second method is to combine equation (4-16) with mass balance equation and solve it numerically. Zeolite membrane experiments are usually carried out at steady state conditions[67]. If we assume one-dimensional permeation we can simplify the mass balance equation to:

$$\text{Rectangular: } \rho q_s \frac{\partial\theta_i}{\partial t} = -\frac{\partial N_{i,z}}{\partial x} \qquad (4\text{-}18)$$

If we introduce equation (4-16) to equation (4-18), the following partial differential equation will be obtained:

$$\rho q_s \frac{\partial\theta_i}{\partial t} = -\frac{\partial}{\partial x}\left(-\rho q_s D_i \frac{1}{1-\theta_i}\frac{\partial\theta_i}{\partial x}\right) \qquad (4\text{-}19)$$

Equilibrium condition is present at both the feed and permeates side. To solve equation (4-19), the following boundary and initial conditions are being used:

$$t = 0,\ 0 \le x \le \Delta X\ ;\ \ \theta_i(x)=0 \qquad (4\text{-}20)$$

$$x = 0; \quad \theta_i(x,t) = \frac{b_i P_{i,f}}{1 + b_i P_{i,f}} \tag{4-21}$$

$$x = \Delta X; \quad \theta_i(x,t) = \frac{b_i P_{i,p}}{1 + b_i P_{i,p}} \ , \tag{4-22}$$

where $P_{i,f}$ and $P_{i,p}$ are partial pressure of component i at the feed and the permeate side, respectively. Figures and modeling result will be presented later in this chapter.

At high temperatures and low pressures adsorption isotherms often approach Henry's regime with adsorbed amounts that are linearly dependent on pressure:

$$q_i = K_i P_i \ , \tag{4-23}$$

where K_i is the Henry's constant of component i. K_i is also dependent on temperature according to the Van't Hoff equation. $K_{i,0}$ is the Henry's constant at reference temperature:

$$K_i = K_{i,0} \exp\left[\left(\frac{\Delta H_i}{R_g}\right)\left(\frac{1}{T_0} - \frac{1}{T}\right)\right] \tag{4-24}$$

Hence, similar to the previous analysis, zeolitic permeance $\Pi_{i,z}$ can be expressed as:

$$\Pi_{i,z} = \frac{N_{i,z}}{\Delta P_i} = \frac{\rho K_{i,0}}{\Delta X} D_{i,0} \exp\left[\left(\frac{E_i^D + \Delta H_i}{R_g}\right)\left(\frac{1}{T_0} - \frac{1}{T}\right)\right] \tag{4-25}$$

The behaviour of surface diffusion mechanism with temperature depends on the values of E_i^D and ΔH_i and loading[69]. When $E_i^D + \Delta H_i > 0$, zeolitic permeance increases as temperature rises, at high temperatures and low pressures.

Based on these equations it is understood that Maxwell-Stefan theory is able to describe both the effect of adsorption and diffusion. Adsorption-diffusion mechanism occurs when one of the components is adsorbed into the pores and diffuses through the membrane by means of surface diffusion. As a result, the other species will be excluded. In this mechanism, gas diffusivity is increasing with temperature; however, its adsorption strength is decreased at elevated thermal conditions which allows the non-adsorbing component to permeate through the membrane[3]. This means diffusion and adsorption are competing with each other which in some cases results in a plateau value for the selectivity over temperature in some of the membranes[44]. In high temperature hydrogen separation processes (over 400 C) the effect of adsorption is negligible and the separation process is mainly controlled by diffusion and molecular sieving[3,70]. Adsorption affinity can be useful in separation of xylene isomers especially p-xylene as it adsorbs stronger than other xylene isomers[62].

Krishna et al. have also shown that Maxwell-Stefan method is successful in predicting mixtures' behaviour in zeolite membranes by using IAST (ideal adsorbed solution theory) or RAST (real adsorbed solution theory) adsorption models[67]. However, in this study we will not discuss multi-component permeance behaviour.

4.3- Flow through non-zeolite pores

Producing a scaled up membrane with uniform pore size is challenging[3]. Usually, there are large pores or defects present in the membrane other than zeolite pores. Gas transport through non-zeolite pores are governed by Knudsen and viscous flux mechanisms. In this study Knudsen numbers observed were in a transitional regime between 0.5 and 1.0. Thus, both Knudsen and viscous mechanisms are considered. The dusty-gas model[71] has been widely used to describe gas-phase transport in many different porous systems. This model, which describes mass transport in multicomponent systems, can be simplified for a single gas flow[72] as a linear combination of Knudsen and viscous contribution. The flux through non-zeolite pores can be expressed as a combination of Knudsen and viscous flux.

4.3.1- Knudsen flux

Knudsen mechanism occurs when the mean free pass of the diffusing molecule is comparable to the membrane pore size. In this case, interactions between the gas molecule and the pore wall of the membrane affect the transport mechanism more than intermolecular interactions. Generally, Knudsen flow plays an important role in H_2/CO_2 separation in membranes with pore sizes higher than 0.5 nm.[3] However as mentioned earlier in this chapter, the Knudsen number (Kn), which is the ratio

of the mean free path to the pore radius ($Kn = \frac{\lambda}{r}$), indicates whether Knudsen diffusion or viscous flow dominates. For Knudsen numbers higher than 10, transport is predominantly driven by Knudsen[65].

If we assume one-dimensional flow, Knudsen flux through a porous media is expressed as:

$$N_{i,k} = -\frac{1}{R_g T} D_{i,Kn} \frac{dP_i}{dx} \ , \tag{4-26}$$

where $D_{i,Kn}$ is Knudsen diffusivity and is described as:

$$D_{i,Kn} = \frac{4}{3} k_0 \sqrt{\frac{8000 R_g T}{\pi M_w}} \ , \tag{4-27}$$

where k_0 is Knudsen structural parameter. If we assume that pores are cylindrical, open ended and non-intersecting, Knudsen diffusion would be expressed as:

$$D_{i,Kn} = \frac{2}{3} r_i \sqrt{\frac{8000 R_g T}{\pi M_w}} = 97\, r_i \sqrt{\frac{T}{M_w}} \ , \tag{4-28}$$

where r_i is the average non-zeolite pore size of the membrane.

4.3.2- Viscous flux

Viscous flow or Hagen-Poiseuille flow is dominant when pore size of the membrane is larger than the mean free path of gas molecules. In this case the molecule can easily pass through the membrane without any serious interaction

with the pore wall. Gas flux is completely viscous for Knudsen numbers less than 0.01.

Viscous flow plays an important role in microfiltration and ultrafiltration. However it is not being considered as a selective flow in zeolite membranes[73]. If we assume one-dimensional flow, viscous flux is expressed as:

$$N_{i,v} = -\frac{1}{R_g T}\frac{B_0 P_m}{\mu}\frac{dP}{dx}\ , \tag{4-29}$$

Where B_0 and P_m are the permeability constant and mean pressure between the feed and the permeate side respectively. μ is the component viscosity and is calculated based on Sutherland's formula[74]:

$$\mu = \mu_0 \left(\frac{a_1}{a_2}\right)\left(\frac{T}{T_0}\right)^{3/2}, \tag{4-30}$$

where μ_0 is gas viscosity at reference temperature and T_0 is the reference temperature. a_1 and a_2 are expressed as:

$$a_1 = 0.555\, T_0 + a_3 \tag{4-31}$$

$$a_2 = 0.555\, T + a_3 \tag{4-32}$$

Parameter a_3 is Sutherland's constant. In this study the values reported by Crane company were used[74]. μ_0 and the reference temperature were found in CRC handbook[75].

Assuming non-intersecting cylindrical pores B_0 can be defined as the following:

$$B_0 = \frac{r_i^2}{8} \tag{4-33}$$

Based on dusty-gas model the flux through non-zeolite pores can be expressed as a combination of Knudsen and viscous flux:

$$N_{i,nz} = -\frac{1}{R_g T}\left(D_{i,Kn} \frac{dP_i}{dx} + \frac{B_0 P_m}{\mu} \frac{dP}{dx} \right) \tag{4-34}$$

By using equations (4-26) and (4-29) and integrating over membrane thickness, we can easily show that non-zeolitic flux can be expressed as below:

$$N_{i,nz} = N_{i,k} + N_{i,v} = \frac{1}{\tau} \frac{1}{\Delta X} 97\, r_i \sqrt{\frac{T}{M_w}} \frac{\Delta P_i}{R_g T} + \frac{1}{\tau} \frac{1}{\Delta X} \frac{r_i^2 P_m}{8\mu} \frac{\Delta P}{R_g T} , \tag{4-35}$$

where the first and second terms represent Knudsen and viscous flows, respectively. As discussed earlier, we have assumed cylindrical and non-intersecting pores in the model. However, in reality they are not perfect. To overcome this issue, τ, the membrane tortuosity, is introduced to consider geometrical effects of pores. τ is defined as the ratio of pore length over thickness of the membrane. It is also assumed that the dominant part of the non-zeolitic gas transport occurs in free-transport pores of cylindrical shape with radii distributed around the mean value $\langle r_i \rangle$.[76]

Thus, total flux through the membrane can be estimated as:

$$N_{i,t} = \propto N_{i,z} + (1 - \propto) N_{i,nz} , \quad \propto = \frac{A_z}{A_t} , \tag{4-36}$$

where $(1-\propto)$ is the fraction of cross sectional area that corresponds to the defects or non-zeolite pores. A_z and A_t are the zeolite open pore area and the total permeable area of the membrane respectively. By introducing equation (4-17) and (4-35) to equation (4-36), total flux through membrane can be described as follows:

$$N_{i,t} = -\propto \frac{\rho q_s D_i}{\Delta X} \ln\left(\frac{1+b_i P_{permeate}}{1+b_i P_{feed}}\right) + \frac{(1-\propto)}{\tau} \frac{1}{\Delta X} 97\, r_i \sqrt{\frac{1}{M_w}} \frac{\Delta P_i}{R_g\sqrt{T}} + \frac{(1-\propto)}{\tau} \frac{1}{\Delta X} \frac{r_i^2 P_m}{8\mu} \frac{\Delta P}{R_g T} \quad (4\text{-}37)$$

The membrane permeance is estimated using the following expressions:

$$\Pi_i = \frac{N_{i,t}}{\Delta P_i} \quad (4\text{-}38)$$

In H_2/CO_2 separation, membrane's ideal selectivity is defined as the ratio of total permeance of H_2 over CO_2:

$$S^i_{H_2/CO_2} = \frac{\Pi_{H_2}}{\Pi_{CO_2}} \quad (4\text{-}39)$$

4.4- Permeation Simulation

4.4.1- Parameter optimization

Considering equation (4-10), (4-15) and (4-37), there are eight parameters that need to be determined in order to model the permeance through the membrane: $\propto, \tau, r_i, D_{i,0}, E_i^D, b_{i,0}, \Delta H_i, q_s$. ΔH_i can be calculated based on Van't Hoff 's

equation (Equation 4-15). Adsorption parameters can be found either from literature or from isotherm analysis (Figure 4.2) and are listed in Table 4.1 for membrane M2.

Table 4.1. Adsorption isotherm parameters for M2 at 298 K

Membrane/Parameter	q_s (mol kg^{-1})	b_i (Pa^{-1})
M2	1.2	0.93×10^{-3}

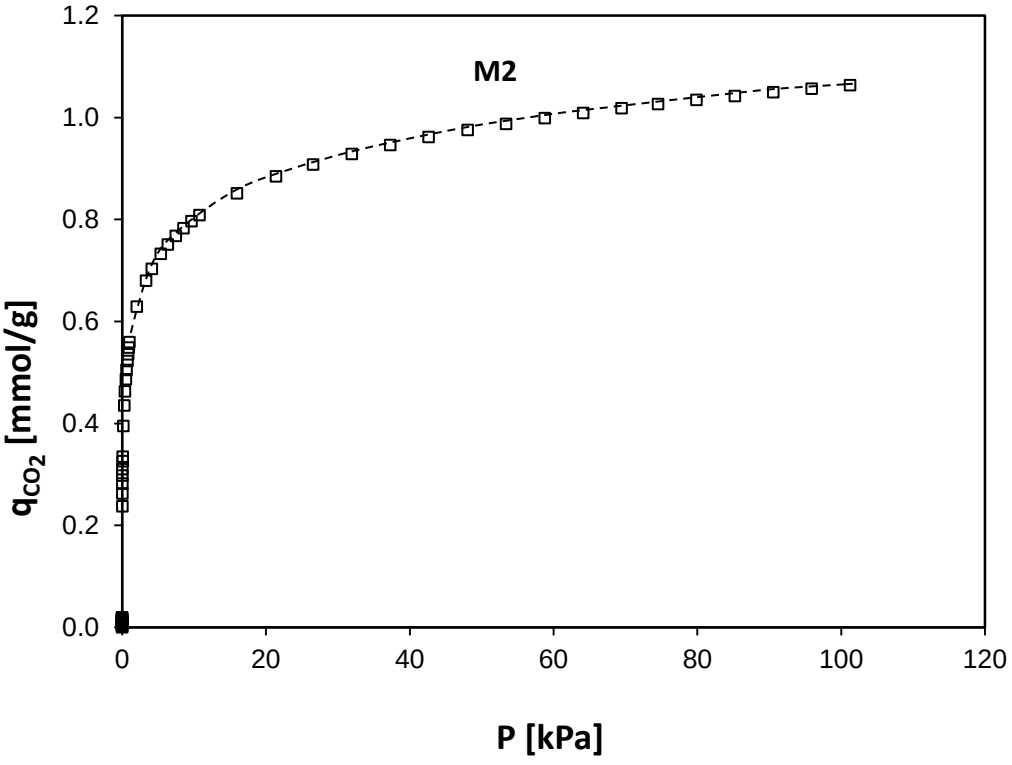

Figure 4.2. CO_2 isotherms for M2 at 298 K.

If equation (4-37) is first fitted at constant temperature and various pressures, there is no need to consider temperature dependency of b_i and diffusivity; in other words we can ignore adjusting E_i^D and ΔH_i. Therefore, with known adsorption parameters and at constant temperature conditions, the parameters that need to be determined are $\propto, \tau, r_i, D_i$. Diffusivity is hard to measure. However, in this study a simple analysis is introduced to estimate the order of diffusivity for H_2 (Section 5.1.3). The other three parameters can be optimized from the fitting process.

Experimental data for H_2 and CO_2 permeances (at temperatures from 298 K to 573 K and feed pressures from 101.35 kPa to 202.7 kPa) were fitted with the model described in the previous section. H_2 and CO_2 fluxes through the membrane can be expressed as a combination of zeolite, Knudsen and viscous flux fractions. The adsorption enthalpy of CO_2 (ΔH_{CO_2}) on membrane M2 was obtained from the adsorption isotherm data at different temperatures (Figure 4.3) using the Van't Hoff equation (Equation 4-15) and was equal to -18 kJ/mol. The H_2 adsorption enthalpy ΔH_{H_2} and activation energies for diffusion of H_2 and CO_2 ($E_{H_2}^D$ and $E_{CO_2}^D$) were optimized estimated values from the fitting process and values reported in literatures for zeolites with similar framework. ΔH_{H_2} was estimated to be -3.0 kJ/mol and $E_{H_2}^D$ and $E_{CO_2}^D$ were calculated to be 10.5 and 21.5 kJ/mol, respectively based on the fitting process. Areán et al.[84] have reported a

value of -3.5 kJ/mol for ΔH_{H_2} in FER zeolite, while Gu et al.[85] have obtained 18.1 kJ/mol for $E_{CO_2}^D$ on MFI zeolite membrane. Kanezashi et al.[86] estimated a value of 9.6 kJ/mol for $E_{H_2}^D$ through DDR zeolite membranes.

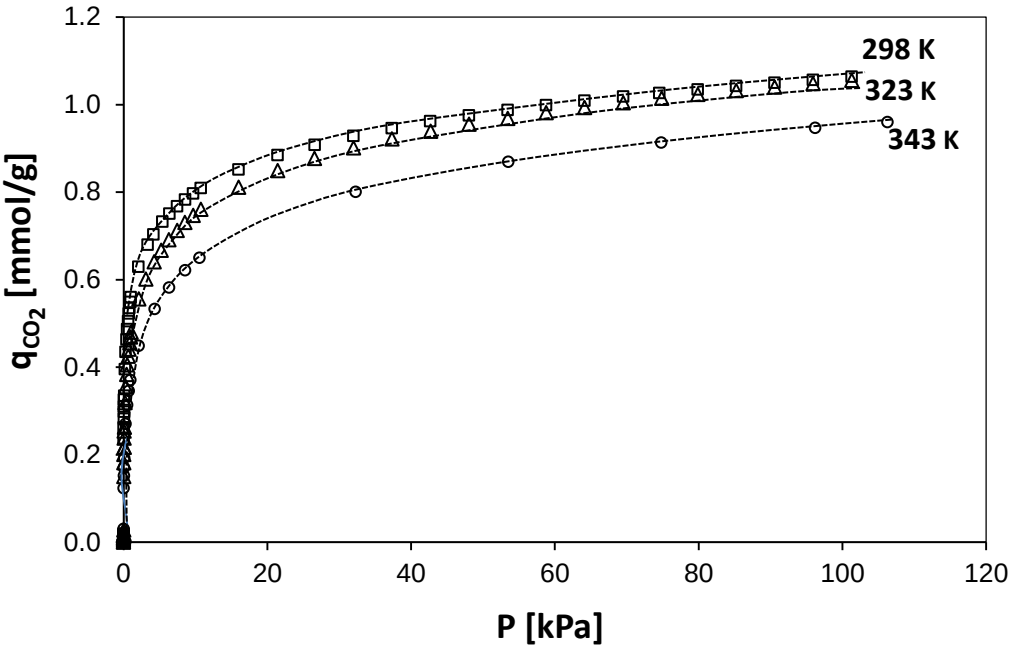

Figure 4.3. CO_2 isotherms for M2 at temperatures 298, 323 and 343K.

To make the fitting process simpler, another technique can be used. For this purpose, different parameters are grouped into three set of parameters. "'Nelder-Mead simplex direct" method was used to optimize the parameters with MATLAB. Objective function is the experimental measured permeance through the membrane. Total flux and optimized parameters A, B and C for the permeation experiments through membrane M2 are defined as follows:

$$N_{i,t} = -A \exp\left[\left(\frac{E_i^D}{R_g}\right)\left(\frac{1}{T_0} - \frac{1}{T}\right)\right] \ln\left(\frac{1+b_i P_{permeate}}{1+b_i P_{feed}}\right) + B\sqrt{\frac{1}{T M_w}}\,\Delta P_i + C\,\frac{P_m}{\mu}\frac{\Delta P}{T} \tag{4-40}$$

$$A = \propto \frac{\rho q_s D_{i,0}}{\Delta X} \tag{4-41}$$

$$B = \frac{1}{\tau}(1-\propto)\frac{2}{3}\frac{\langle r_i \rangle}{\Delta X}\sqrt{\frac{8000}{\pi R_g}} \tag{4-42}$$

$$C = \frac{1}{\tau}(1-\propto)\frac{1}{\Delta X}\frac{\langle r_i^2 \rangle}{8 R_g} \tag{4-43}$$

Optimizing these parameters against different temperature and pressure conditions can help us to understand membranes better and compare different membrane with each other. In this section, permeation modeling for a membrane, made from natural deposits from British Columbia in Canada, is presented. Experimental data for H_2 and CO_2 permeances (at temperatures from 298 K to 573 K and feed pressures from 101.35 kPa to 202.7 kPa) were fitted with the model described in this chapter. Optimized parameters for H_2 and CO_2 permeation through this membrane (M2) are summarized in Table 4.2. Value of parameter A, related to the zeolite diffusion flux, is lower for CO_2 than for H_2. This is primarily associated with the lower diffusivity (D_i) of CO_2. The value of parameter B, associated with Knudsen diffusion is smaller for CO_2 than H_2. One explanation for this could be the possible reduction of Knudsen diffusivity as adsorption strength increases, as reported by Krishna et al.[68] However, this explanation deserves more discussion. The value of the parameter C (related to viscous flux) is the same for

H_2 and CO_2 since it depends only on the membrane characteristics and not on the gas type.

Table 4.2. Values of the model parameters for membrane M2

Gas type/Parameter	***A*** (mol m^{-2} s)	***B*** (mol K J^{-1})$^{0.5}$	***C*** (mol K m J^{-1})
H_2	2.84×10^{-3}	1.62×10^{-6}	1.25×10^{-15}
CO_2	1.52×10^{-5}	8.67×10^{-7}	1.25×10^{-15}

4.4.2- Estimation of the contributions of different transport mechanisms

H_2 Permeation modelling at different temperature against pressure is shown in figures 4.4 to 4.7. Fitting parameter values are from Table 4.2.

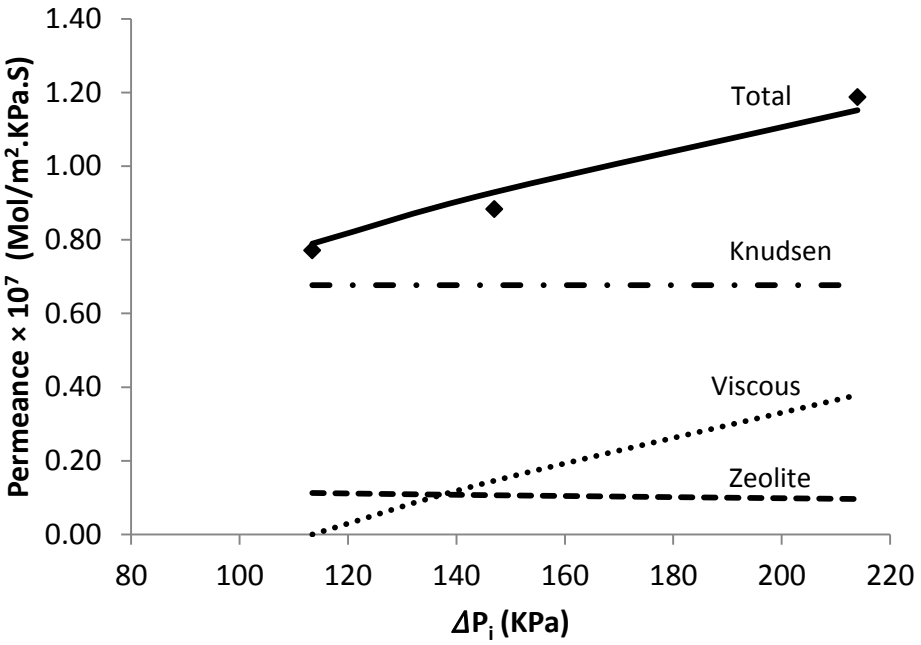

Figure 4.4. Contribution of the transport mechanisms to total H_2 permeance as a function of pressure at 298 K across membrane M2. The diamond represents experimental measurements.

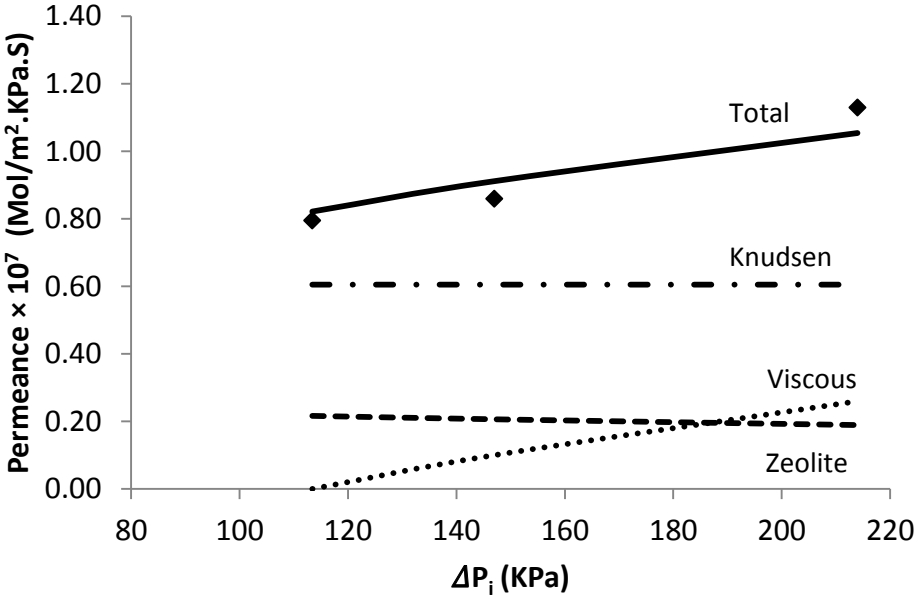

Figure 4.5. Contribution of the transport mechanisms to total H_2 permeance as a function of pressure at 373 K across membrane M2. The diamond represents experimental measurements.

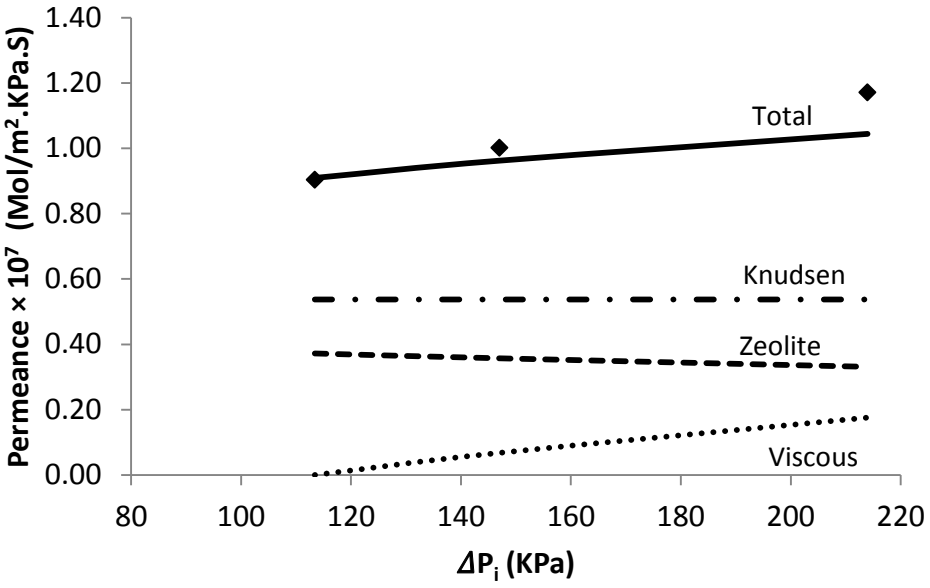

Figure 4.6. Contribution of the transport mechanisms to total H_2 permeance as a function of pressure at 473 K across membrane M2. The diamond represents experimental measurements.

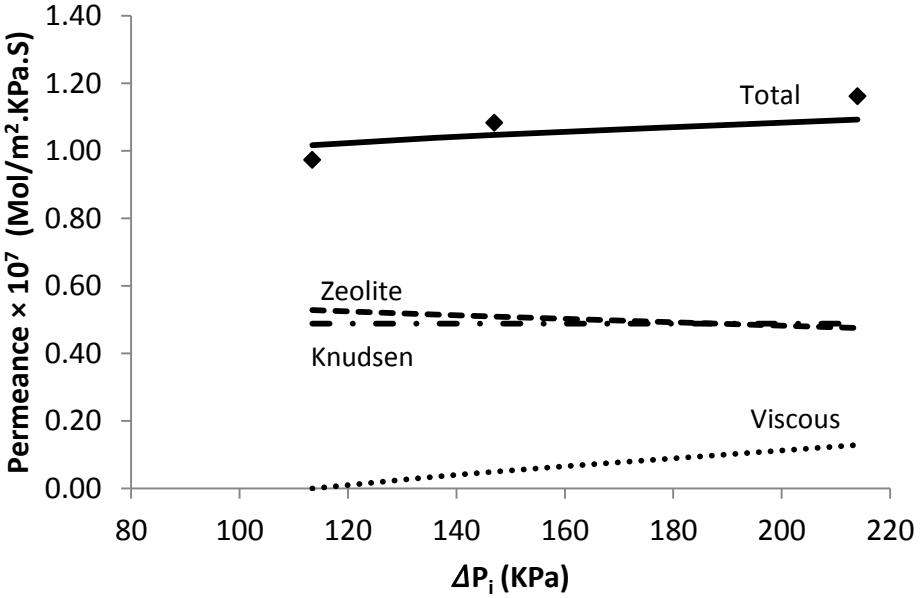

Figure 4.7. Contribution of the transport mechanisms to total H_2 permeance as a function of pressure at 573 K across membrane M2. The diamond represents experimental measurements.

It can be observed from figures 4.3 to 4.6 that the transport model reasonably fits with the experimental data. Viscous flow increases with an increase in pressure. The reason is that by increasing partial pressure difference across the membrane, more gas can flow through the relatively larger pores or membrane defects. Knudsen flux is constant with pressure as expressed in equation (4-26). Zeolite permeance decreases slightly with pressure. However, because permeance is defined as the flux over partial pressure difference, zeolitic permeance decreases with pressure. The figures show that Knudsen and viscous contributions decrease with temperature. However, zeolite permeance increases with temperature. This fact is more pronounced in modelling of permeance against temperature at different pressures. The behaviour of different transport mechanisms against temperature is summarised in Figures 4.8 to 4.10.

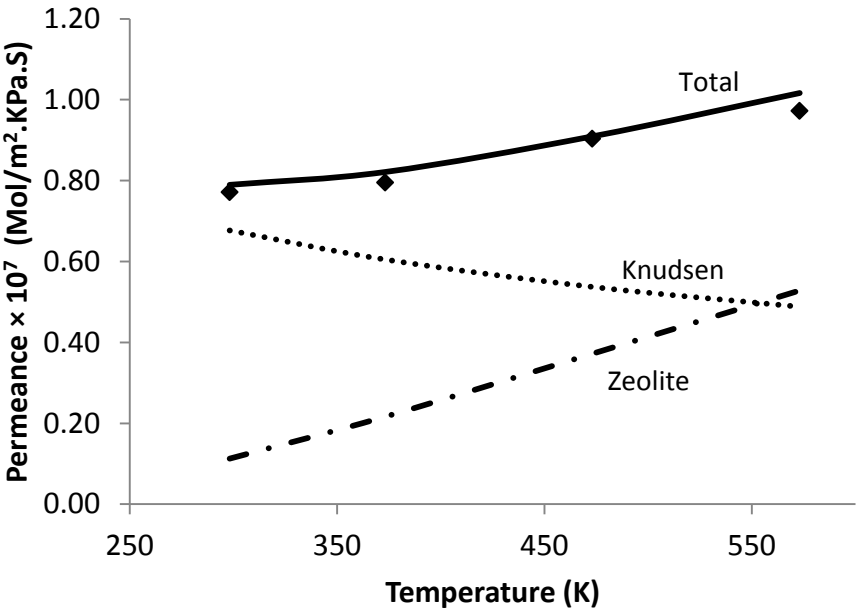

Figure 4.8. Contribution of the transport mechanisms to total H_2 permeance as a function of temperature across membrane M2. Feed and permeate pressures are equal to 101.3 kPa. The diamond represents experimental measurements.

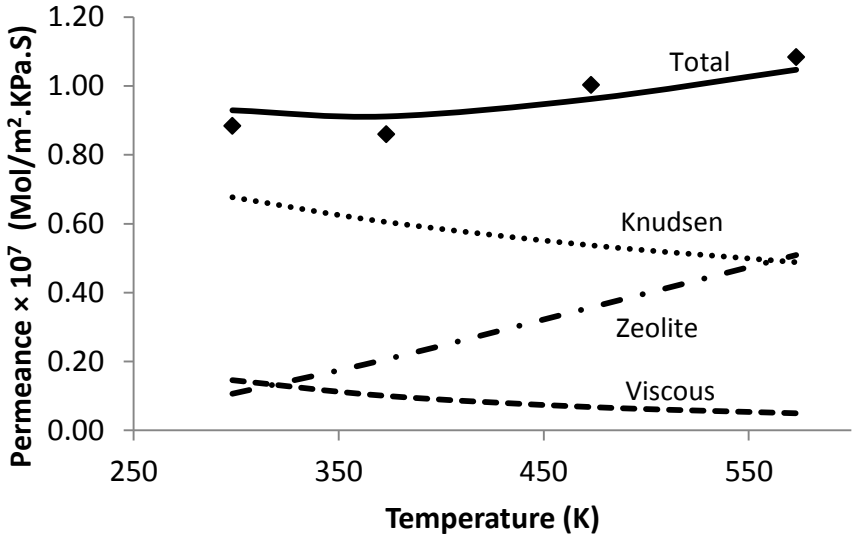

Figure 4.9. Contribution of the transport mechanisms to total H_2 permeance as a function of temperature at feed pressure of 135.8 kPa and permeate pressure of 101.3 kPa across membrane M2. The diamond represents experimental measurements.

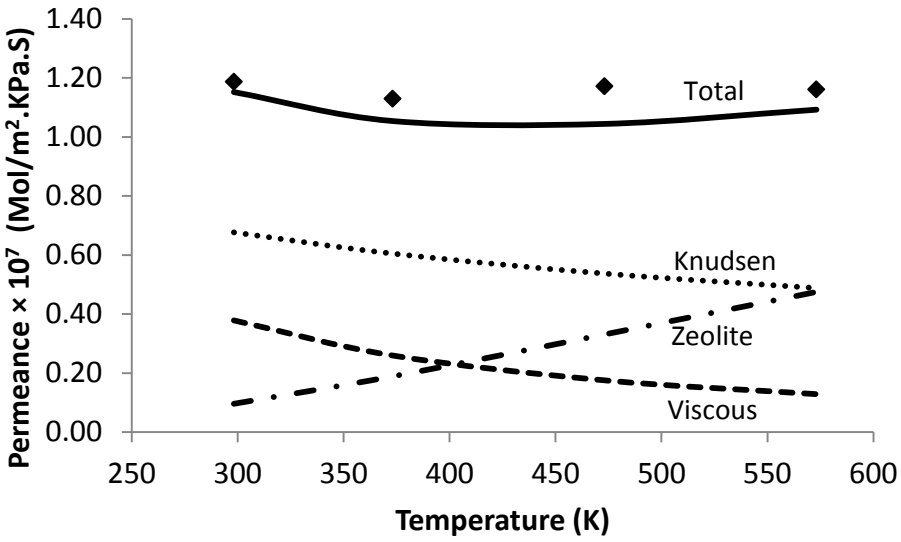

Figure 4.10. Contribution of the transport mechanisms to total H_2 permeance as a function of temperature at feed pressure of 202.7 kPa and permeate pressure of 101.3 kPa across membrane M2. The diamond represents experimental measurements.

Figures 4.8 to 4.10 show that the total permeance of hydrogen increases with temperature due to the effect of temperature on the zeolitic flux. Zeolitic permeance increases with temperature due to the increase in hydrogen molecule diffusion rate through the membrane as discussed earlier according to Maxwell-Stefan theory. This phenomenon compensates for the decrease in adsorption rate of hydrogen molecules due to an increase in temperature as discussed in section 4.2.

CO_2 permeance modeling versus temperature and pressure are shown in figures 4.11 to 4.16. The same analyses are valid for the effect of temperature and pressure on different kinds of CO_2 transport mechanisms through the membrane.

Lower zeolitic contribution was observed in CO_2 permeation modeling. This might be because of lower diffusivity of CO_2 compared with H_2.

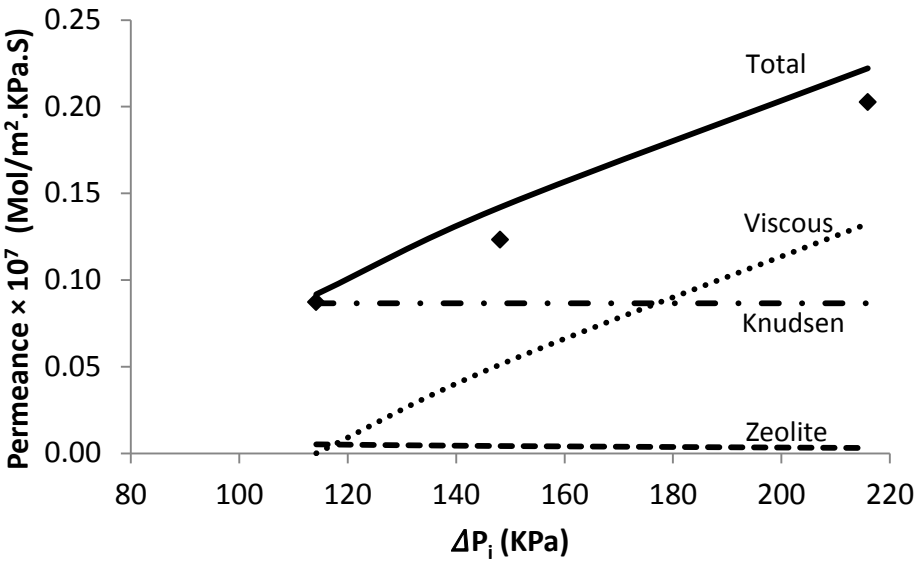

Figure 4.11. Contribution of the transport mechanisms to total CO_2 permeance as a function of pressure at 298 K across membrane M2. The diamond represents experimental measurements.

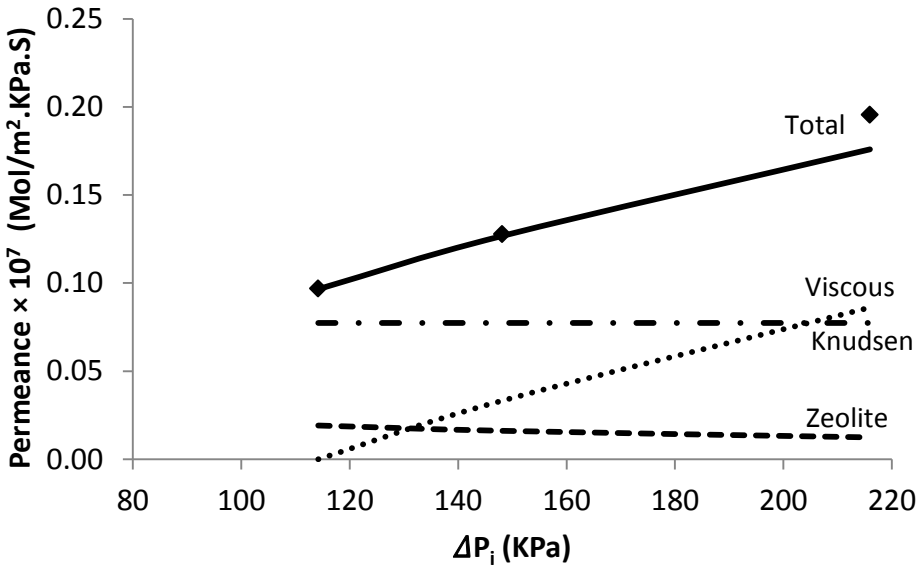

Figure 4.12. Contribution of the transport mechanisms to total CO_2 permeance as a function of pressure at 373 K across membrane M2. The diamond represents experimental measurements.

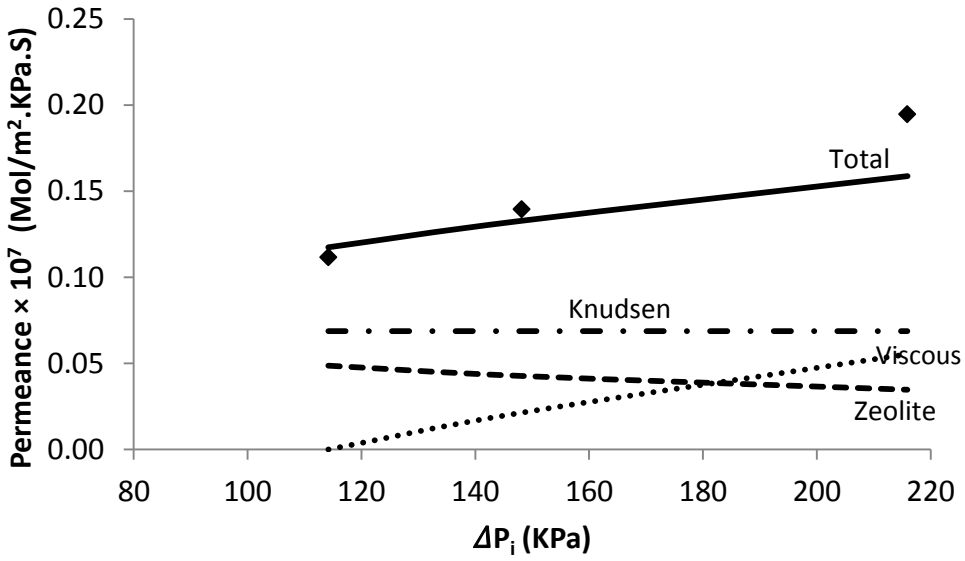

Figure 4.13. Contribution of the transport mechanisms to total CO_2 permeance as a function of pressure at 473 K across membrane M2. The diamond represents experimental measurements.

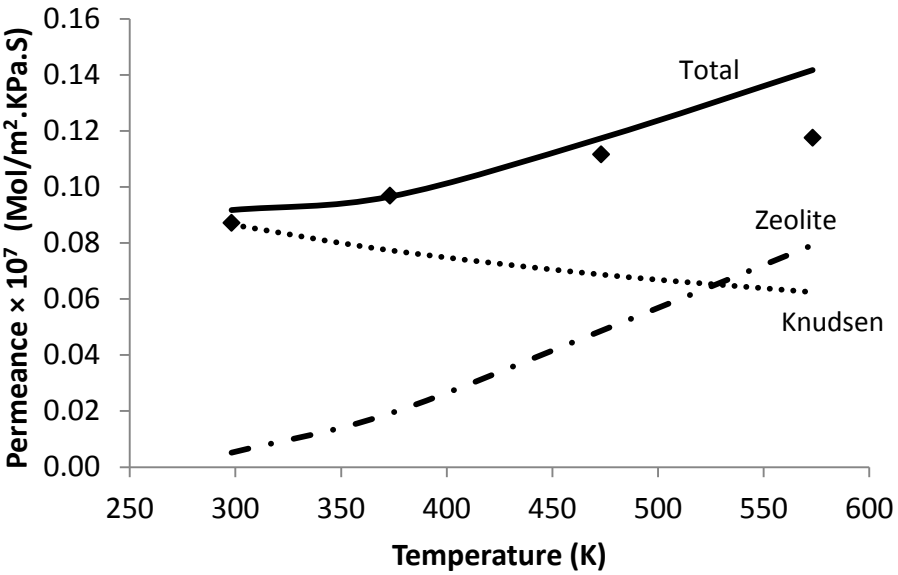

Figure 4.14. Contribution of the transport mechanisms to total CO_2 permeance as a function of temperature across membrane M2. Feed and permeate pressures are equal to 101.3 kPa. The diamond represents experimental measurements.

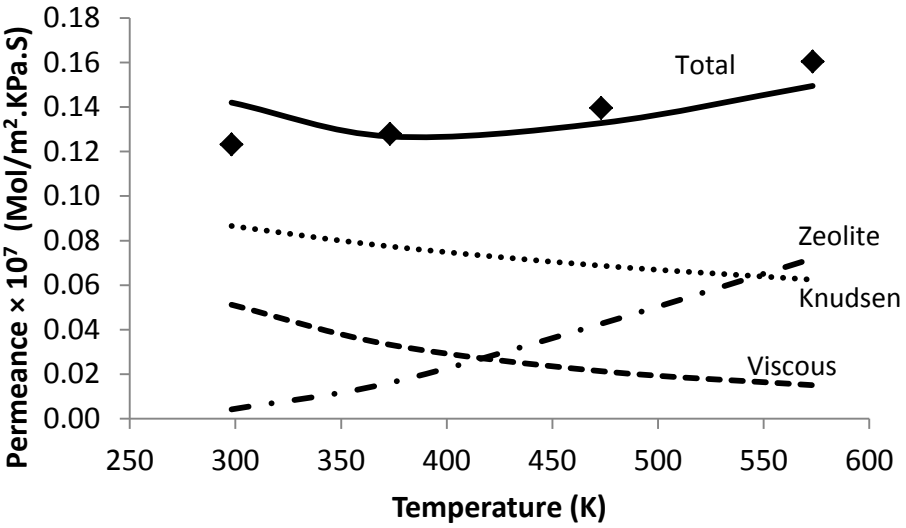

Figure 4.15. Contribution of the transport mechanisms to total CO_2 permeance as a function of temperature at feed pressure of 135.8 kPa and permeate pressure of 101.3 kPa across membrane M2. The diamond represents experimental measurements.

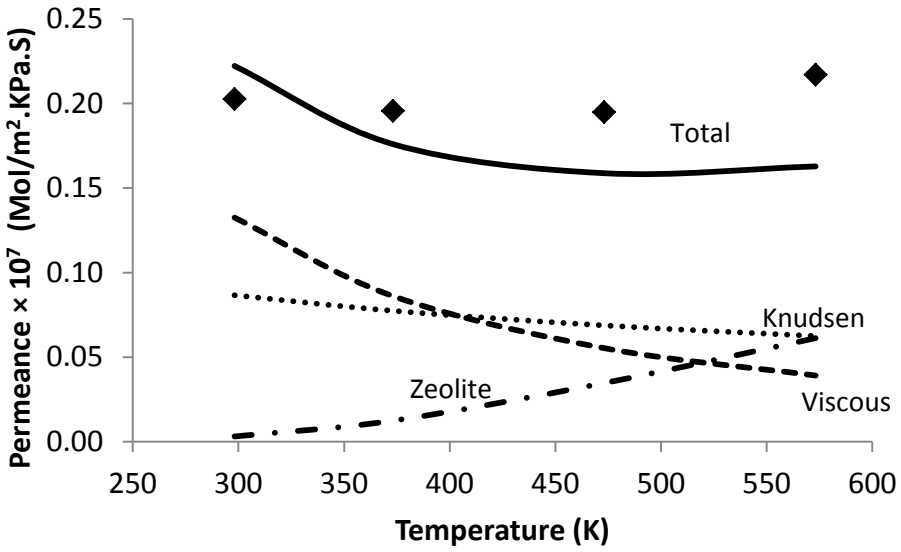

Figure 4.16. Contribution of the transport mechanisms to total CO_2 permeance as a function of temperature at feed pressure of 135.8 kPa and permeate pressure of 202.7 kPa across membrane M2. The diamond represents experimental measurements.

Some deviations are observed at higher pressure and temperature conditions especially for CO_2. One of the reasons for this behaviour might be the under-estimation of defect flow at high pressure and temperature conditions. Miachon et al.[77] have proposed that the intercrystalline area of the membrane increases with temperature which results in an increase in non-zeolite flux.

4.4.3- Numerical Modeling approach

By using numerical methods to solve equation (4-19), more information can be obtained on the functionality of zeolitic permeance with time and the distance passed through the membrane (x). Figure 4.17 shows simulation of H_2 zeolitic

permeance versus x and t at both the permeate and the feed side for membrane M2 at 298 K and zero pressure difference across the membrane. A 3D view of this simulation is presented in figure 4.18.

The steady state time is around 60 S for H_2 permeance at 298 K. It is worth noting that we are solving equation (4-19) and showing the behaviour of zeolite flux only and not the total permeance through the membrane. If we plot permeance versus time at different temperatures, we could compare the effect of temperature on steady state time of the permeance through one membrane. Figure 4.19 shows this analysis for hydrogen permeance through Membrane M2. This figure shows that an increase in temperature results in lower steady state time for the permeance.

The effect of temperature on steady state time is more pronounced for CO_2 zeolitic permeances. Figure 4.20 shows CO_2 permeance against time at different temperatures and zero pressure difference. It can be seen that CO_2 permeance steady state time decreases with temperature more than H_2. This means that CO_2 has higher activation energy compared to H_2. This observation can help us in permeation modelling and parameter optimization. In addition, it appears that CO_2 has a bigger steady state time than H_2 due to its lower diffusivity. However, in an actual testing membrane, due to the presence of defects and large pores, different transient flux profiles are expected. Diffusion times through non-zeolite pores are shorter in comparison to those in zeolite crystals. This will result in shorter steady state time.

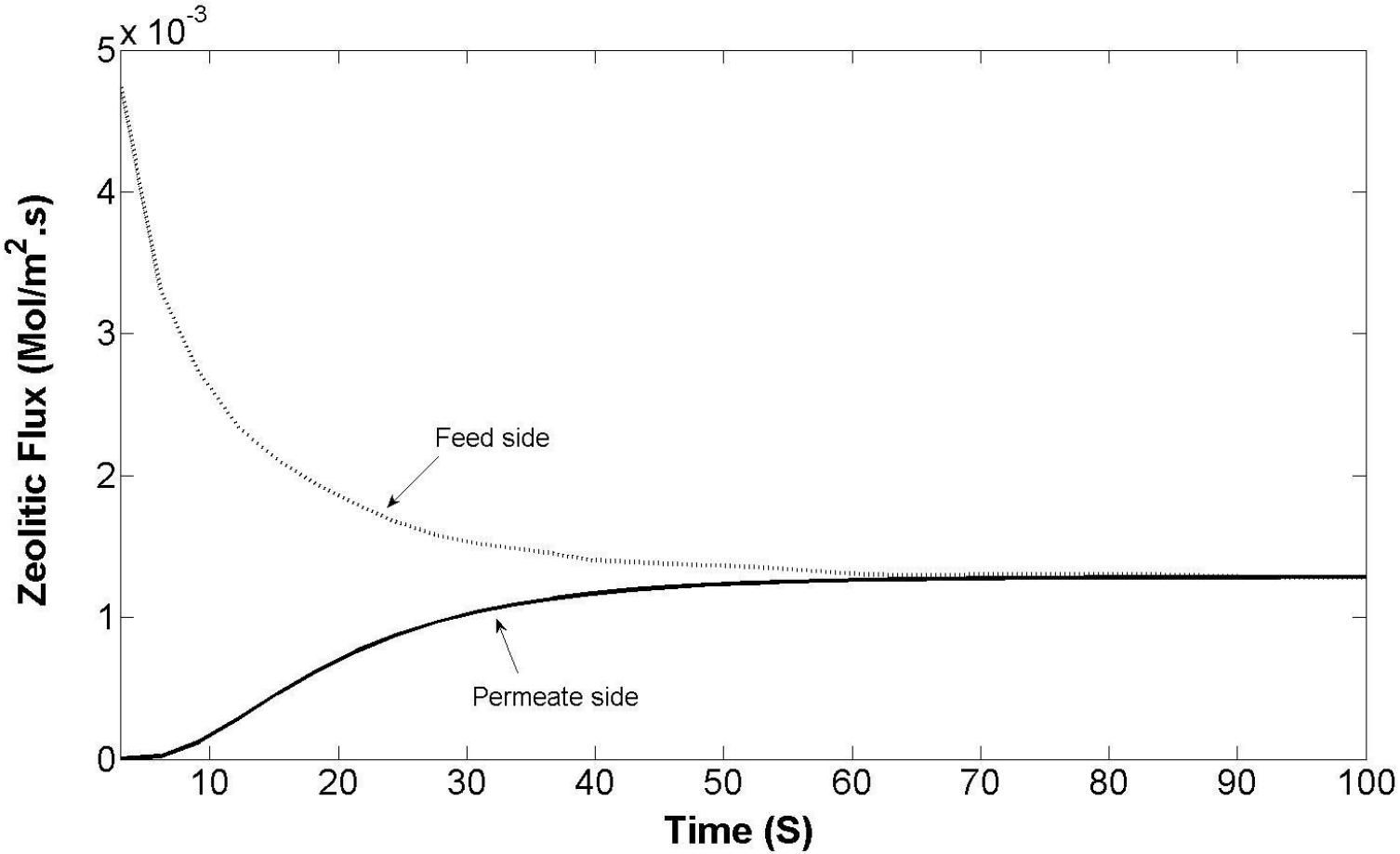

Figure 4.17. H_2 Zeolitic flux at the permeate and the feed side as a function of time across membrane M2 at 298 K and feed and permeate pressure of 101.3 kPa.

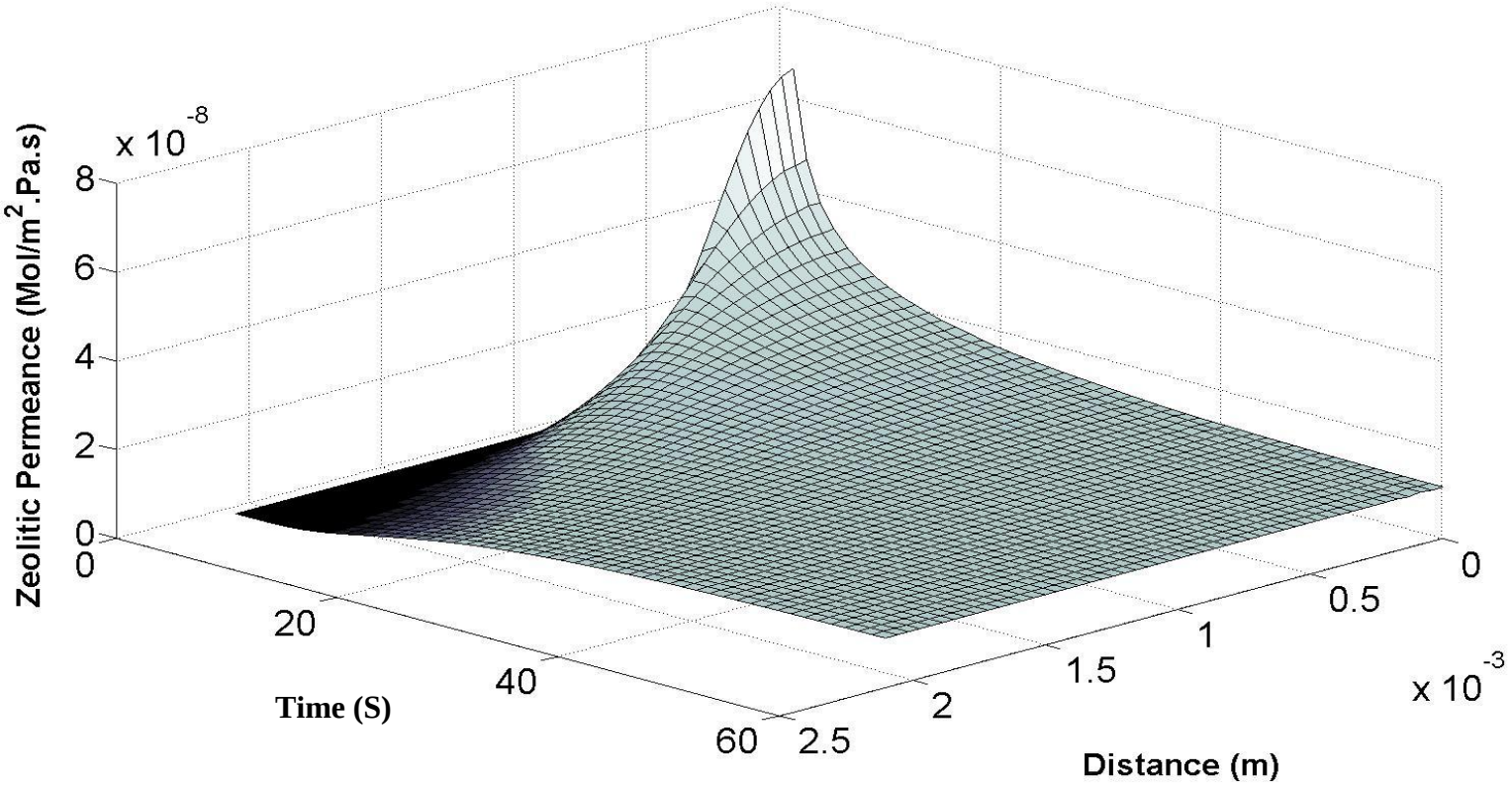

Figure 4.18. H_2 Zeolitic permeance as a function of time and distance across membrane M2 at 298 K and feed and permeate pressure of 101.3 kPa.

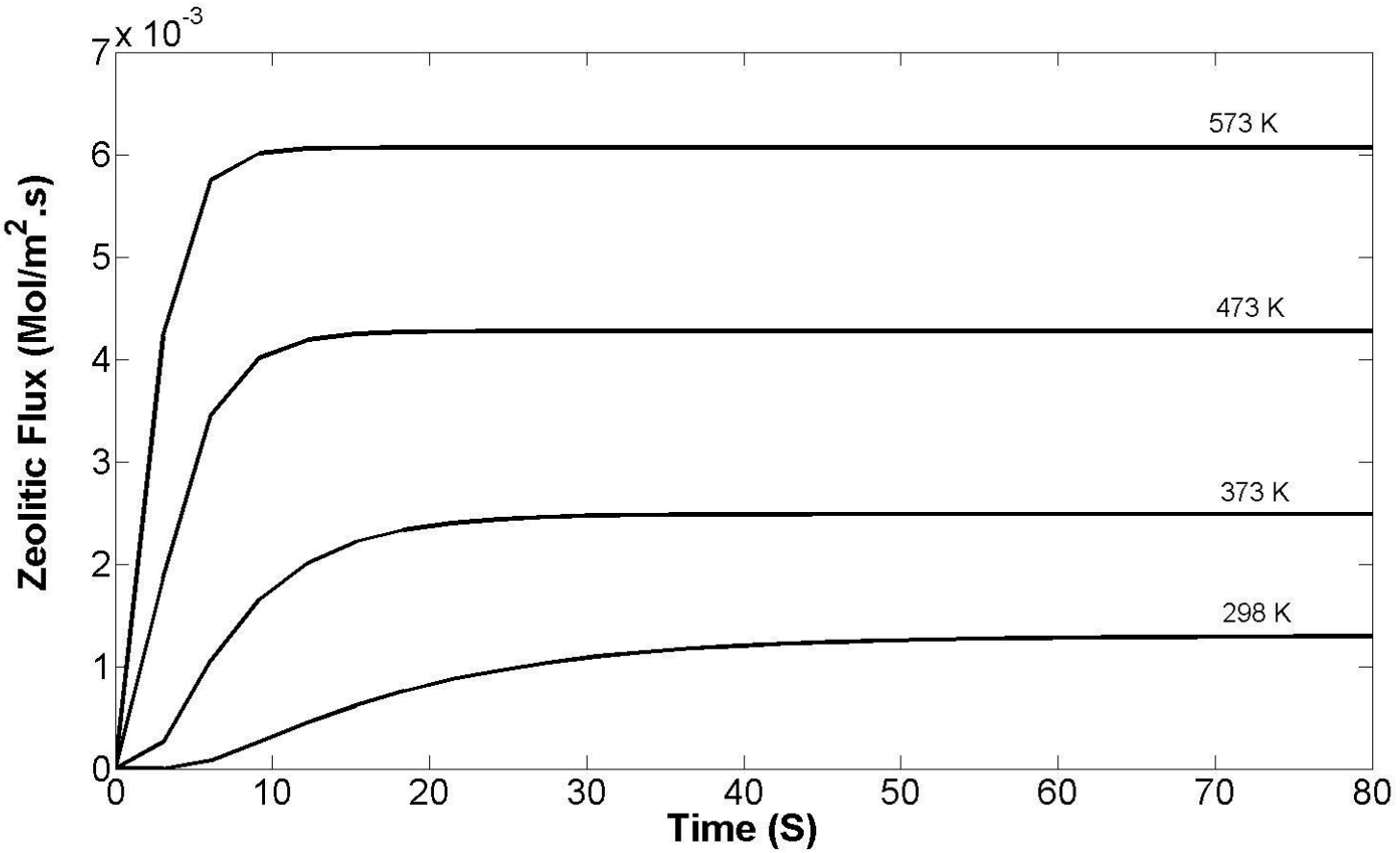

Figure 4.19. Effect of temperature on steady state time of H_2 Zeolitic flux across membrane M2 at feed and permeate pressure of 101.3 kPa.

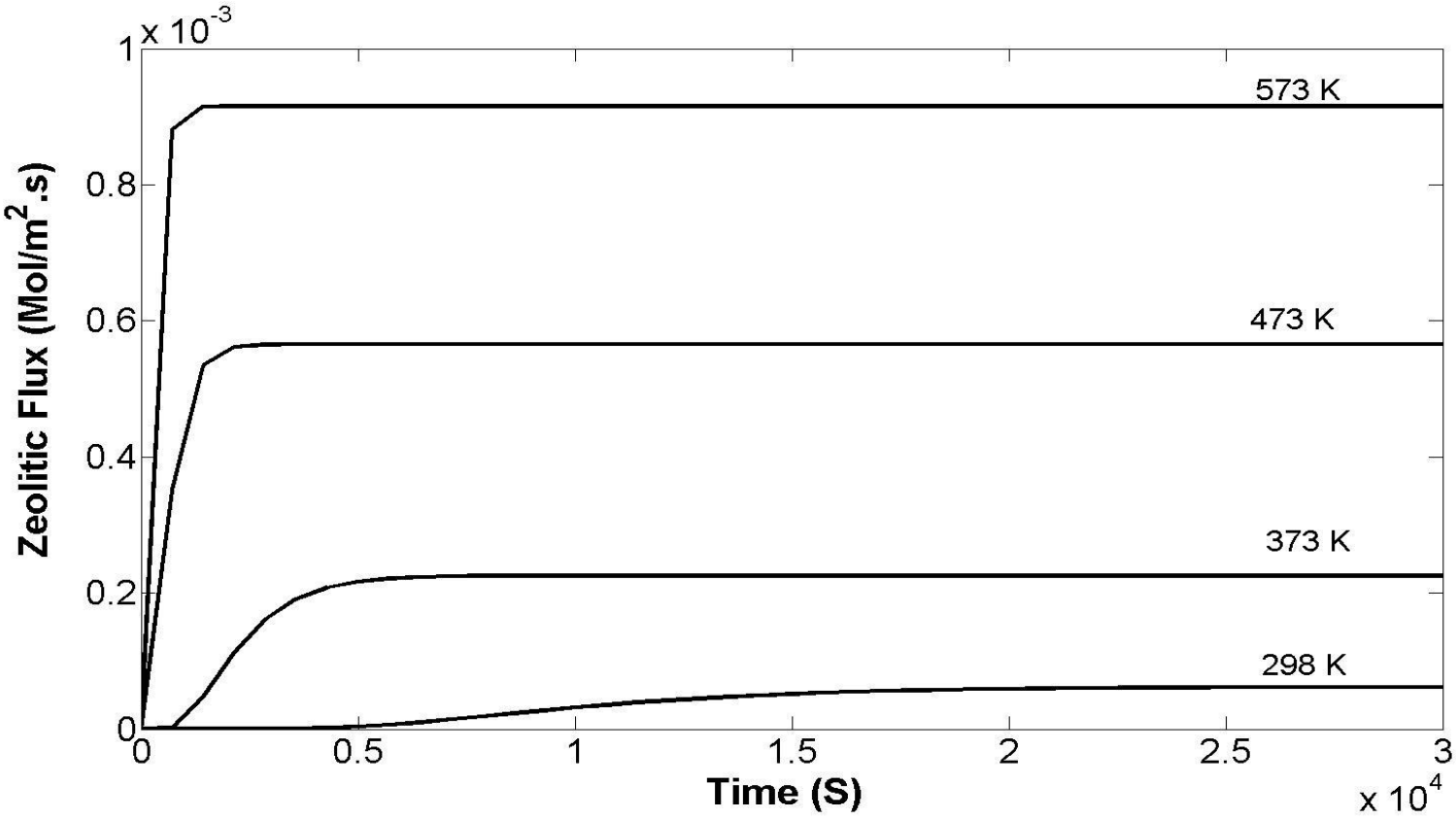

Figure 4.20. Effect of temperature on steady state time of CO_2 Zeolitic flux across membrane M2 at feed and permeate pressure of 101.3 kPa

The effect of pressure on the permeance steady state time was also studied. This analysis is presented in figures 4.21 and 4.22 for H_2 and CO_2 respectively. According to the data pressure does not have a significant effect on the steady state time of the permeance through the membrane. Another observation is that the slope of H_2 permeance at the beginning is steeper than CO_2. This might be due to the stronger adsorption affinity of CO_2 compared to H_2 which helps CO_2 to stick to the zeolite pores.

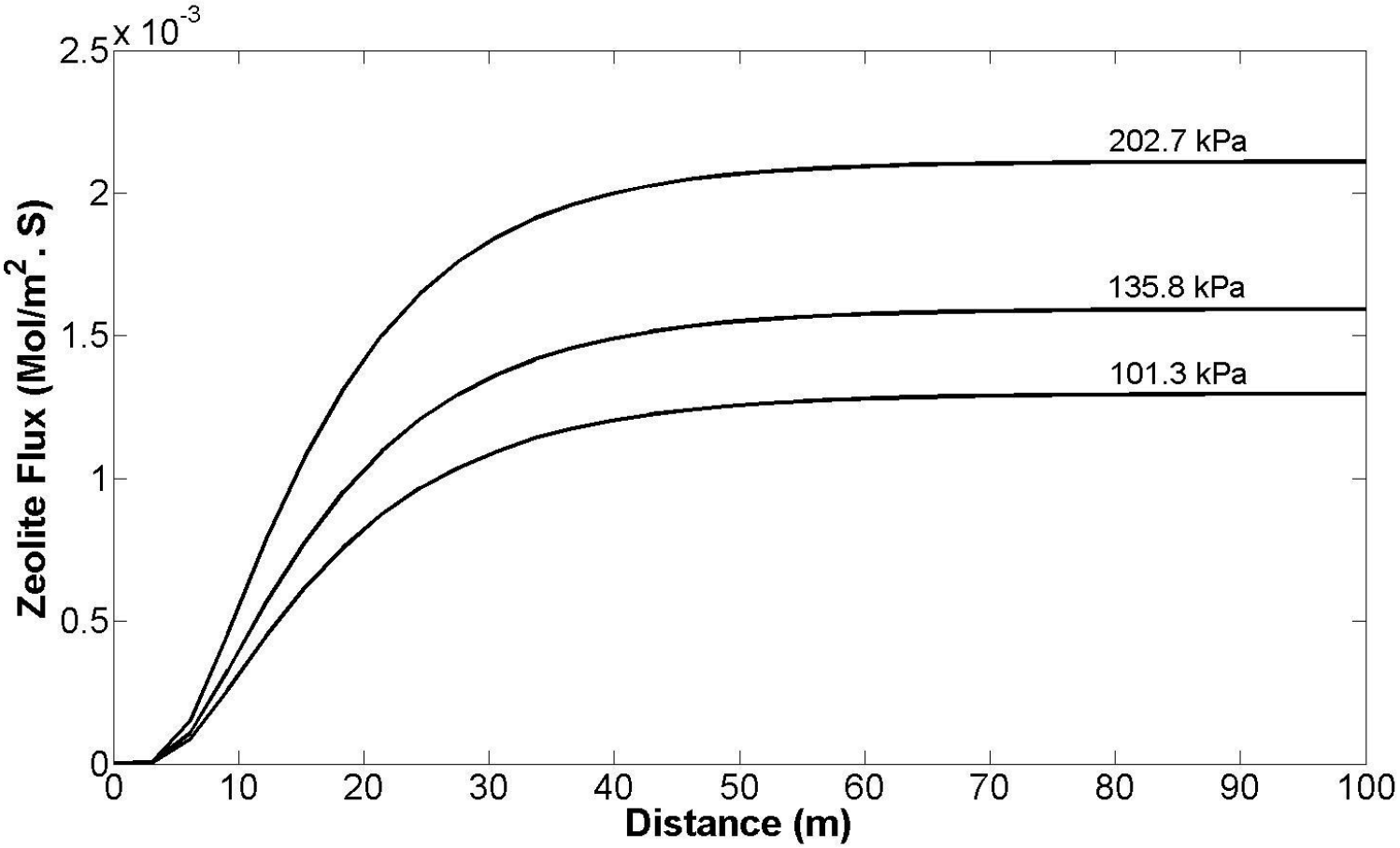

Figure 4.21. Effect of pressure on steady state time of H_2 Zeolitic flux across membrane M2 at 298 K.

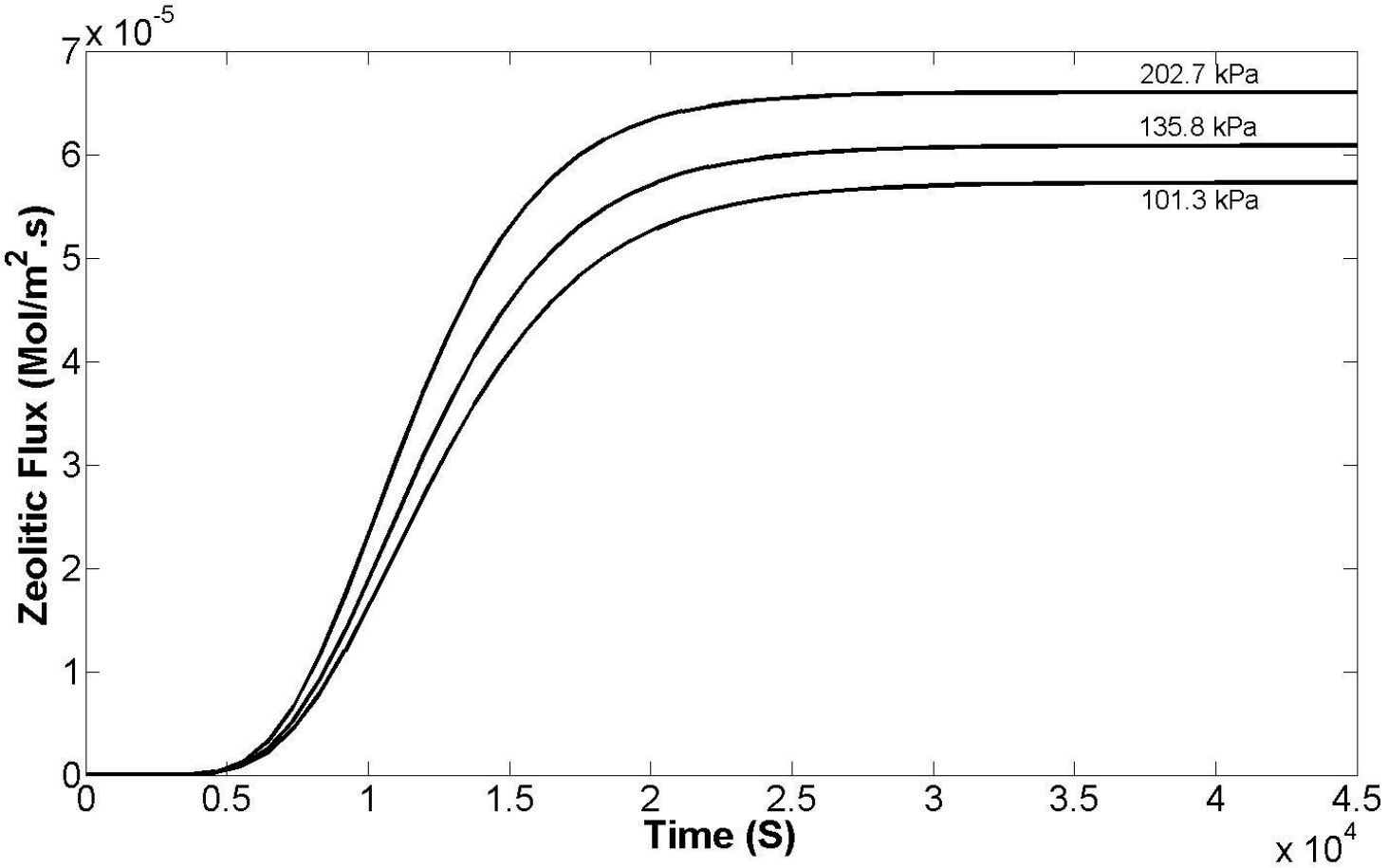

Figure 4.22. Effect of pressure on steady state time of CO_2 Zeolitic flux across membrane M2 at 298 K.

Chapter 5. Model Application on the Characterization of Natural Zeolite Membranes*

5.1- Membrane Characterization

5.1.1- Comparative parameter analyses based on relative average pore size

As discussed earlier in chapter four, permeance through natural zeolite membranes is assumed to be a combination of zeolitic, Knudsen and viscous flow contributions. Equation (4-37) can be rearranged as follows:

$$\Pi_{i,t}\,\Delta X = \frac{N_{i,t}}{\Delta P_i}\Delta X = -\propto \frac{\rho q_s D_i}{\Delta P_i}\,\ln\left(\frac{1+b_i P_{permeate}}{1+b_i P_{feed}}\right) + \frac{(1-\propto)}{\tau}\,97\langle r_i\rangle\sqrt{\frac{T}{M_w}}\,\frac{1}{R_g T} + \frac{(1-\propto)}{\tau}\,\frac{\langle r_i^2\rangle P_m}{8\mu}\,\frac{1}{R_g T}\,\frac{\Delta P}{\Delta P_i} \quad (5\text{-}1)$$

The right side of the above equation is permeability that is the permeance multiplied by thickness of the membrane. $\langle r_i\rangle$ is the integral mean of defect radii distribution.

According to equation (5-1) H_2 permeability at 298 K across the membrane can be considered as a combination of two terms based on pressure functionalities. One fraction (Poiseuille or viscous contribution) is dependent on pressure while

* A version of this chapter has been submitted for publication to the journal of Industrial & Engineering Chemistry Research (ACS Publications).

the other (Knudsen and zeolitic contributions) is not. Then, the permeability of H_2 can be expressed as:

$$Permeability = \alpha_v [P^*] + \beta_{kz}, \quad (5\text{-}2)$$

$$P^* = P_m \frac{\Delta P}{\Delta P_i} \quad (5\text{-}3)$$

The first term in equation (5-2) is pressure dependent while the second term is not. P_m is the arithmetic mean pressure between the feed and the permeate stream. Based on equations (5-1) and (5-2), α_v and β_{kz} are the slope and intercept of a linear fitting of the permeability data as a function of P^* and are expressed as:

$$\alpha_v = \frac{1}{\tau}\left(1 - \frac{A_z}{A_t}\right) \frac{\langle r_i^2 \rangle}{8\mu} \frac{1}{R_g T} \quad (5\text{-}4)$$

$$\beta_{kz} = \frac{1}{\tau}\left(1 - \frac{A_z}{A_t}\right) 97 \langle r_i \rangle \sqrt{\frac{T}{Mw}} \frac{1}{R_g T} + \left[- \left(\frac{A_z}{A_t}\right) \frac{\rho q_s D_i}{\Delta P_i} \ln\left(\frac{1 + b_i P_{permeate}}{1 + b_i P_{feed}}\right)\right] \quad (5\text{-}5)$$

Lin and Burgraaf[78] have shown that the ratio $\frac{\alpha_v}{\beta_{kz}}$ is a comparative parameter related to the medium pore size of different membrane. The membrane with the smallest non-zeolite pore size corresponds to the lowest value of the $\frac{\alpha_v}{\beta_{kz}}$ ratio. However, they studied the effect of pore size reduction on He permeability in alpha-alumina membranes. In their study, the total permeability was considered as a contribution of Knudsen and viscous flux. However, the total flux through the zeolite-based membranes includes the intrinsic zeolite flux in addition to the non-zeolite fluxes (equation (5-5)). In this chapter it will be shown that $\frac{\alpha_v}{\beta_{kz}}$ is a parameter attributed to membrane defect size in zeolite-based membranes, if

$(\frac{\alpha_v}{\beta_{kz}})_{M_2} > (\frac{\alpha_v}{\beta_{kz}})_{M_1}$ and $(\alpha_v)_{M_2} < (\alpha_v)_{M_1}$. α_v has a quadratic dependence on defect radii of the non-zeolite pores while β_{kz} is a linear function of the defect radii. We can characterize membrane's defect size by plotting permeability as a function of P^*.

For membranes having a defect size distribution, the permeation flux can be expressed as:

$$N_{i,t} = \frac{A_z}{A_t} N_{i,z} + \frac{1}{\tau A_t} \int_{r_k > r_z}^{\infty} N_{i,nz}(r_k)\, a_i(r_k)\, n(r_k)\, dr_k \tag{5-6}$$

where $N_{i,nz}(r_k)$ is the permeation flux through a pore of radius r_k which is larger than the zeolite pore size($r = r_z$); $a_i(r_k)$ is the cross-sectional area of each pore of radius r_k and $n(r_k)$ is the number pore size distribution which is related to the area pore size distribution, $\eta(r_k)$, through the following equation[78]:

$$\eta(r) = \frac{a_i(r_k)\, n(r_k)}{A_i} \ , \tag{5-7}$$

where A_i is the non zeolitic area of the membrane. Using equation (5-7) in equation (5-6), the permeation flux of a membrane having a defect size distribution is:

$$N_{i,t} = \frac{A_z}{A_t} N_{i,z} + \frac{1}{\tau}\left(1 - \frac{A_z}{A_t}\right) \int_{r_k > r_z}^{\infty} N_{i,nz}(r_k)\ \eta(r_k)\, dr_k \tag{5-8}$$

By using the corresponding equations for Knudsen, viscous and intracrystalline transport mechanisms (equations (4-29), (4-32) and (4-17) respectively), the permeability can be expressed as:

$$Permeability = \frac{N_{i,t}\,\Delta x}{\Delta P_i} = \alpha_v\, P^* + \beta_{kz} \tag{5-9}$$

where the parameters α_v and β_{kz} are expressed as:

$$\alpha_v = \frac{1}{\tau}\left(1 - \frac{A_z}{A_t}\right)\frac{\langle r_i^2\rangle}{8\mu}\,\frac{1}{R_g T} \tag{5-10}$$

$$\beta_{kz} = \underbrace{\frac{1}{\tau}\left(1 - \frac{A_z}{A_t}\right)\,97\,\langle r_i\rangle\sqrt{\frac{T}{Mw}}\,\frac{1}{R_g T}}_{\gamma = Knudsen\ contribution} + \underbrace{\left[-\left(\frac{A_z}{A_t}\right)\frac{\rho q_s D_i}{\Delta P_i}\,\ln\left(\frac{1+b_i P_{permeate}}{1+b_i P_{feed}}\right)\right]}_{\psi = Zeolite\ contribution} \tag{5-11}$$

$\langle r_i\rangle$ is the integral mean of defect radii distribution and is expressed as:

$$\langle r_i\rangle = \int_{r_k > r_z}^{\infty} r_k\ \eta(r_k)\, dr_k \tag{5-12}$$

And $\langle r_i^2\rangle$ is the integral mean of distribution of squared defect radii and can be described by the following:

$$\langle r_i^2\rangle = \int_{r_k > r_z}^{\infty} r_k^2\ \eta(r_k)\, dr_k \tag{5-13}$$

The terms γ and ψ in equation (5-11) represent the permeabilities associated with Knudsen and zeolitic flow, respectively. In this analysis it is shown that ψ is independent of pressure and membrane type. Because of the weak adsorption affinity of H_2 , its zeolite flux is almost constant at 298 K for different feed pressures. Therefore, ψ can be assumed to be independent of pressure. $\frac{A_z}{A_t}$ is a

value that approaches one (not equal to one) and its relative variation for different membranes is essentially negligible. The rationale is related to the fact that Knudsen diffusivities are much higher than zeolite crystal diffusivities. Therefore, only a very small fraction of membrane area is required to provide a large contribution of non-zeolite flux. Hence, in general for normal quality zeolite membranes the zeolite open pore area over total permeable area ratio $\frac{A_z}{A_t}$ is a value that approximates to one[89]. In particular, the model fit values for the parameter $\alpha=\frac{A_z}{A_t}$ fall into the range $0.99 > \alpha > 1$ for the evaluated membranes in this work. This means that the factor $\frac{A_z}{A_t}$ essentially does not modify the magnitudes of ψ term as estimated for different membranes. As we consider adsorption parameters of the same order for different rocks from a single deposit, ψ can be considered to be constant for different batches in this characterization analysis.

Thus, under these assumptions, for H_2 permeance through M1 and M2 where M1 and M2 are two different membranes with the same zeolite material, if $(\frac{\alpha_v}{\beta_{kz}})_{M_2} > (\frac{\alpha_v}{\beta_{kz}})_{M_1}$:

$$(\frac{\alpha_v}{\beta_{kz}})_{M_2} > (\frac{\alpha_v}{\beta_{kz}})_{M_1} \Longrightarrow (\frac{\alpha_v}{\gamma+\Delta})_{M_2} > (\frac{\alpha_v}{\gamma+\Delta})_{M_1}$$

$$\Longrightarrow (\alpha_v)_{M_2}\,\gamma_{M_1} + (\alpha_v)_{M_2}\,\psi > (\alpha_v)_{M_1}\,\gamma_{M_2} + (\alpha_v)_{M_1}\,\psi \qquad (5\text{-}14)$$

If $(\alpha_v)_{M_2} < (\alpha_v)_{M_1}$:

$$(\alpha_v)_{M_2}\,\psi < (\alpha_v)_{M_1}\,\psi \qquad (5\text{-}15)$$

Using equation (5-15) in equation (5-14) one can easily obtain:

$$(\alpha_v)_{M_2}\,\gamma_{M_1} > (\alpha_v)_{M_1}\,\gamma_{M_2} \Longrightarrow \left(\frac{\alpha_v}{\gamma}\right)_{M_2} > \left(\frac{\alpha_v}{\gamma}\right)_{M_1} \tag{5-16}$$

Replacing equations (5-10) and (5-11) in equation (5-16), it can be shown that:

$$\left[\frac{\langle r_i^2\rangle}{\langle r_i\rangle}\right]_{M_2} \frac{1}{97\times 8\,\mu}\sqrt{\frac{Mw}{T}} > \left[\frac{\langle r_i^2\rangle}{\langle r_i\rangle}\right]_{M_1} \frac{1}{97\times 8\,\mu}\sqrt{\frac{Mw}{T}} \Longrightarrow \left[\frac{\langle r_i^2\rangle}{\langle r_i\rangle}\right]_{M_2} > \left[\frac{\langle r_i^2\rangle}{\langle r_i\rangle}\right]_{M_1}$$

$$\Longrightarrow (r_m)_{M_2} > (r_m)_{M_1}\ , \tag{5-17}$$

where $r_m = \frac{\langle r_i^2\rangle}{\langle r_i\rangle}$ is defined as the flow averaged defect size. Another simple explanation for this is that ψ is not a function of P^*. Therefore, $\frac{\alpha_v}{\beta_{kz}} \approx \frac{\alpha_v}{\gamma}$ at constant temperature. In case of uniform pore membranes:

$$\langle r_i\rangle = r_i\ , \tag{5-18}$$

$$\langle r_i^2\rangle = r_i^2 \tag{5-19}$$

$$\text{And}\ \ r_m = \frac{\langle r_i^2\rangle}{\langle r_i\rangle} = r_i \tag{5-20}$$

Then from equation (5-16):

$$\left(\frac{\alpha_v}{\gamma}\right)_{M_2} > \left(\frac{\alpha_v}{\gamma}\right)_{M_1} \Longrightarrow (r_i)_{M_2}\ \frac{1}{97\times 8\,\mu}\sqrt{\frac{Mw}{T}} > (r_i)_{M_1}\ \frac{1}{97\times 8\,\mu}\sqrt{\frac{Mw}{T}} \Longrightarrow (r_i)_{M_2} > (r_i)_{M_1} \tag{5-21}$$

According to equations (5-17) and (5-21), $\frac{\alpha_v}{\beta_{kz}}$ is a useful parameter for characterizing the membrane defect size in zeolite-based membranes.

Figure 5.1 shows the permeability of three membranes as a function of P^*. M1 shows the highest permeability. The corresponding values of $\frac{\alpha_v}{\beta_{kz}}$ for each membrane are listed in Table 5.1. M2 has a slightly higher value for $\frac{\alpha_v}{\beta_{kz}}$ ratio than M1. This value for M3 is higher compared to the other two membranes, which means M3 might have larger defects. In this chapter we will focus on comparing membranes M1 and M2. The values of $\frac{\alpha_v}{\beta_{kz}}$ for M1 and M2 are interpreted to mean that even though M1 has higher permeability, the average defect size is slightly larger for M2 than for M1.

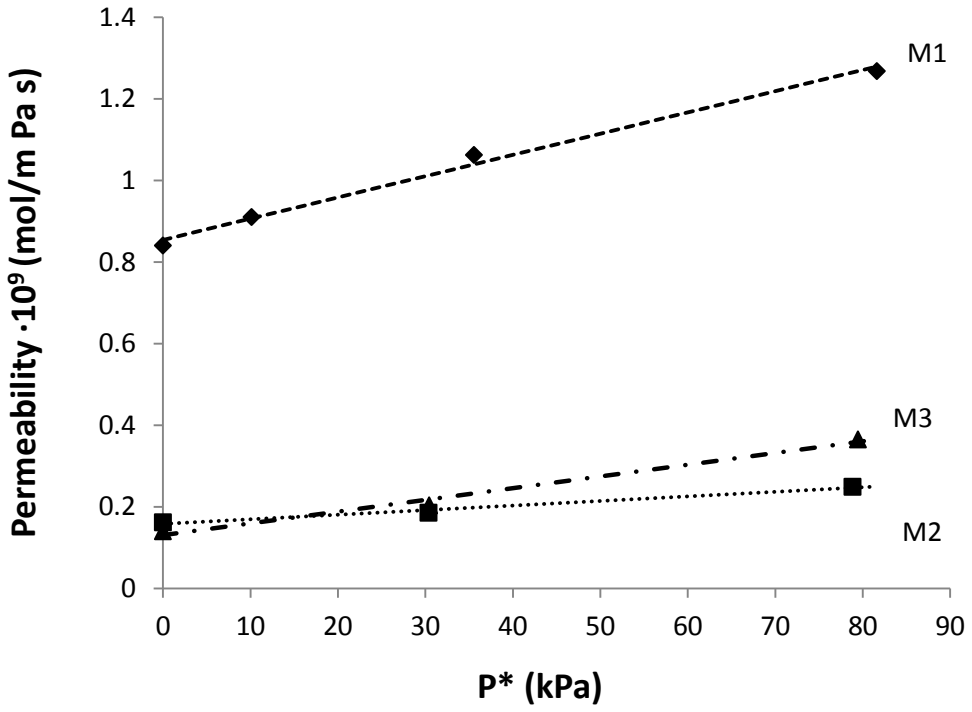

Figure 5.1. H_2 Permeability as a function of P* at 298 K.

Table 5.1. Comparative parameter $\frac{\alpha_v}{\beta_{kz}}$ for membranes M1, M2 and M3 at 298 K

Membrane	M1	M2	M3
α_v x10^{12} (mol m^{-1} s^{-1} kPa^{-2})	5.21	1.12	3.00
β_{kz} x10^{10} (mol m^{-1} s^{-1} kPa)	8.54	1.58	1.00
$\frac{\alpha_v}{\beta_{kz}}$ x10^{3} (kPa^{-1})	6.10	7.09	30

A comparison of relative average defect sizes (Table 5.1) is consistent with the experimental values of the H_2/CO_2 ideal selectivities as the pressure increases at room temperature for both M1 and M2. Figure 5.2 shows the effect of pressure on ideal selectivity for both membranes. Both H_2/CO_2 selectivities were higher than the corresponding Knudsen selectivity ($S^{Kn}_{H_2/CO_2} = \sqrt{\frac{Mw_{CO_2}}{Mw_{H_2}}} = 4.7$). H_2/CO_2 selectivity decreases as the feed pressure increases. The fraction of the "non-selective" viscous flux passing through the relatively larger non-zeolite pores increases as the total pressure drop rises. However, the selectivity of M2 decreased faster with pressure than the selectivity of M1. This means that M2 might have higher contribution of viscous flow at higher pressures that causes a decrease in its selectivity at elevated pressures. This is consistent with a larger defect size for M2 as compared to M1: $\left(\left[\frac{\alpha_v}{\beta_{kz}}\right]_{M2} > \left[\frac{\alpha_v}{\beta_{kz}}\right]_{M1}\right)$.

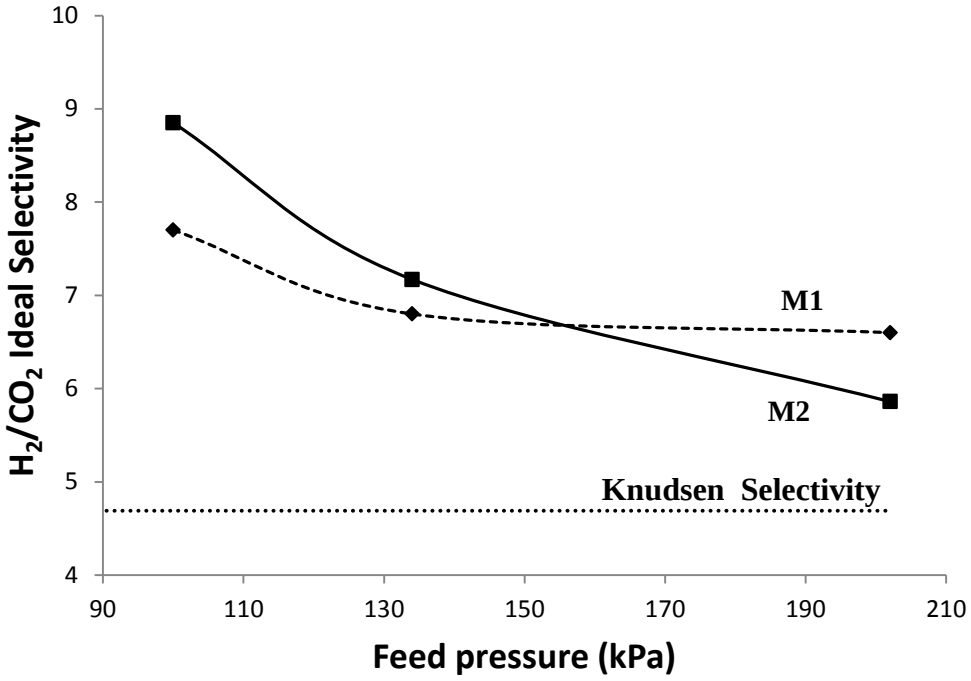

Figure 5.2. H_2/CO_2 ideal selectivity as a function of the feed pressure on the untreated natural zeolite membranes at 298 K.

5.1.2- Comparative parameter analyses based on non-zeolitic area

To characterize the membrane defect size we plot permeability versus P* (Figure 5.1). The linear function, its slope (α_v) and intercept (β_{kz}) are defined by equations (5-9), (5-10) and (5-11), respectively. Ratio $\frac{\alpha_v}{\beta_{kz}}$ can be used to characterize the membrane defect size. We introduce another parameter, $\frac{{\beta_{kz}}^2}{\alpha_v}$, that could also be very valuable in characterization of uniform pore membranes. From Equation (5-11) it can be easily shown that:

$$\beta^2 = \gamma^2 + \psi^2 + 2\gamma\psi \qquad (5\text{-}22)$$

The second and third term of this expression can be neglected in comparison to γ^2 as zeolite flow (which is related to ψ) is negligible at 298 K for H_2. As a result, $\beta^2 = \gamma^2$ and:

$$\frac{{\beta_{kz}}^2}{\alpha_v} = \frac{\gamma^2}{\alpha} = \frac{97^2\left(\frac{1}{\tau}\right)^2\left(1-\frac{A_z}{A_t}\right)^2 r_i^2 \frac{T}{Mw}\frac{1}{R_g^2T^2}}{\left(\frac{1}{\tau}\right)\left(1-\frac{A_z}{A_t}\right)\frac{r_i^2}{8\mu}\frac{1}{R_gT}} = 97^2\left(\frac{1}{\tau}\right)\left(1-\frac{A_z}{A_t}\right)\frac{8\mu}{R_gMw} \qquad (5\text{-}23)$$

Right side of equation (5-23) can be written as a constant (φ), which only depends on the viscosity and molecular weight of the permeating gas multiplied by non-zeolitic area of the membrane ($1-\frac{A_z}{A_t}$). We can rewrite equation (5-23) as:

$$\frac{{\beta_{kz}}^2}{\alpha_v} = \left(\frac{1}{\tau}\right)\left(1-\frac{A_z}{A_t}\right)\varphi\ , \qquad (5\text{-}24)$$

$$\varphi = 97^2\frac{8\mu}{R_g Mw} \qquad (5\text{-}25)$$

Thus, $\frac{{\beta_{kz}}^2}{\alpha_v}$ is an additional parameter attributed to the non-zeolitic area of each membrane and the corresponding tortuosity. This parameter characterizes the non-zeolitic area of membrane and is proportional to $\left(1-\frac{A_z}{A_t}\right)$. The $\frac{{\beta_{kz}}^2}{\alpha_v}$ values were calculated for the membranes listed in Table 5.2.

Table 5.2. Comparative parameter $\frac{\beta_{kz}{}^2}{\alpha_v}$ for membranes M1 and M2 at 298 K

Membrane	M1	M2
α_v x10^{12} (mol m^{-1} s^{-1} kPa^{-2})	5.21	1.12
β_{kz} x10^{10} (mol m^{-1} s^{-1} kPa)	8.54	1.58
$\frac{\beta_{kz}{}^2}{\alpha_v}$ x10^3 (mol m^{-1} s^{-1})	14.00	2.23
Density (kg m^{-3})	1,940	2,540

It is worth noting that membrane M1 has a significantly larger $\frac{\beta_{kz}{}^2}{\alpha_v}$ coefficient than M2. M2 comes from a mineral sample with 30% higher density than M1. Thus, a lower $\frac{\beta_{kz}{}^2}{\alpha_v}$ value for M2 can be associated with a higher density of its source rock compared to M1. A high rock density implies a smaller number of defects per membrane unit area. Membrane M2 has a lower defect area than M1 and a higher tortuosity.

5.1.3- Comparative parameter analyses based on permeation data at zero pressure drop

In this study, a third comparative parameter analysis was introduced. This analysis is similar to the other two parameter studies but the conclusion is drawn

from the results of single permeation experiments of H_2 at different temperatures and zero pressure difference instead of room temperature and different pressures. With no pressure difference between feed and permeate side, only zeolite and Knudsen flux contributions can be assumed to be present while there is no viscous flux[79]. The overall H_2 flux through the membrane can be expressed as (Equation 4-37):

$$N_{i,t} = -\frac{A_z}{A_t}\frac{\rho q_s D_i}{\Delta X}\ln\left(\frac{1+b_i P_{permeate}}{1+b_i P_{feed}}\right) + \frac{1}{\tau}\left(1-\frac{A_z}{A_t}\right)\frac{97}{\Delta X}\langle r_i\rangle\sqrt{\frac{1}{Mw}}\frac{\Delta P_i}{R_g\sqrt{T}} \quad (5\text{-}26)$$

The first and the second term correspond to zeolite and Knudsen flow, respectively. Equation (5-26) can be rearranged to:

$$\frac{N_{i,t}\,\Delta x}{\Delta P_i}\sqrt{T} = -\frac{A_z}{A_t}\rho q_s D_{i,0}\,\frac{exp\left[\left(\frac{E_i^D}{R}\right)\left(\frac{1}{T_0}-\frac{1}{T}\right)\right]\sqrt{T}}{\Delta P_i}\,ln\left(\frac{1+b_i P_{permeate}}{1+b_i P_{feed}}\right)$$

$$+\frac{1}{\tau}\frac{A_i}{A_t}\,97\langle r_i\rangle\sqrt{\frac{1}{Mw}}\frac{1}{R_g}, \quad (5\text{-}27)$$

Equation (5-27) can be further simplified to:

$$Permeability\cdot\sqrt{T} = \omega\cdot C + \lambda, \quad (5\text{-}28)$$

where ω and λ are the slope and intercept of a plot of "Permeability $\cdot\sqrt{T}$" versus C. ω, λ and C can be expressed as:

$$\omega = \frac{A_z}{A_t}\rho q_s D_{i,0} \quad (5\text{-}29)$$

$$\lambda = \frac{1}{\tau}\frac{A_i}{A_t}\ 97\langle r_i\rangle\sqrt{\frac{1}{Mw}}\frac{1}{R_g} \tag{5-30}$$

$$C = -\frac{exp[\left(\frac{E}{R}\right)\left(\frac{1}{T_0}-\frac{1}{T}\right)]\ \sqrt{T}}{\Delta P_i}\ ln\left(\frac{1+b_i\,P_{permeate}}{1+b_i\,P_{feed}}\right) \tag{5-31}$$

Figure 5.3 shows the corresponding plot of equation (5-28):

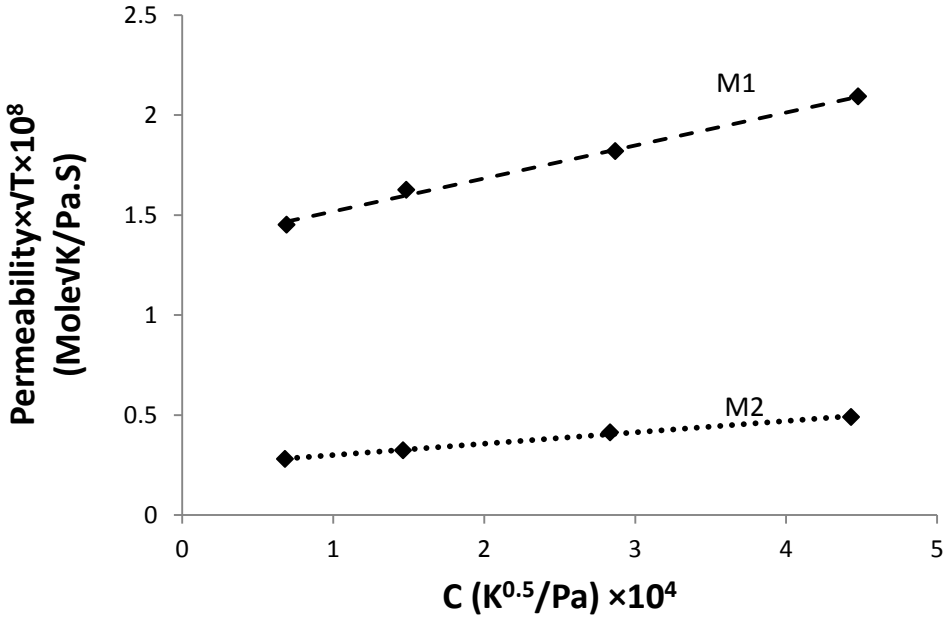

Figure 5.3. H_2 Permeability×√T vs. C.

The ratio $\frac{\lambda}{\omega}$ is proportionate to the coefficient $\frac{1}{\tau}\cdot\frac{A_i}{A_z}\cdot\langle r_i\rangle$. This ratio is related to both average defect size and fractional area of defects (non-zeolite pores). Table 5.3 shows the corresponding values for the coefficient $\frac{\lambda}{\omega}$ for membranes M1 and M2:

Table 5.3. Comparative parameter $\frac{\lambda}{\omega}$ for membranes M1 and M2 at 298 K

Membrane	M1	M2
λ x10^8 (mol $K^{0.5}$ m^{-1} s^{-1} pa^{-1})	1.00	0.2
ω x10^5 (mol m^{-1} s^{-1})	2.00	0.6
$\frac{\lambda}{\omega}$ x10^4 ($K^{0.5}$ Pa)	5.00	3.33

According to Table 5.3, M2 has a smaller value of the coefficient $(\frac{1}{\tau} \cdot \frac{A_i}{A_z} \cdot \langle r_i \rangle)$ compared to M1. The comparison of values of $\frac{\boldsymbol{\alpha_v}}{\boldsymbol{\beta_{kz}}}$ for M1 and M2 (Table 5.1) reflected the fact that $\langle r_i \rangle$ is larger for M2. Therefore, the value of $(\frac{1}{\tau} \cdot \frac{A_i}{A_z})$ for M2 should be much lower than for M1, reflecting a smaller defect area and/or larger tortuosity. This is consistent with the permeability analysis at different pressures and the values obtained for $\frac{{\beta_{kz}}^2}{\alpha_v}$.

In addition to these comparative parameter analyses, profiles of "Permeability $\cdot$ $\sqrt{T}$ " versus C can provide information on diffusion coefficients. The assessment of diffusivities in zeolite crystals is not a trivial issue[80]. However, the order of diffusivity can be estimated from the coefficient $\omega = \frac{A_z}{A_t}\ \rho q_s D_{H_2,0}$. Since $\frac{A_z}{A_t}$ is a value approaching one, and ρq_s approaches ~ 200 $\frac{mol}{m^3}$ in the natural zeolites that were used in this study, the order of magnitude of $D_{H_2,0}$ (diffusivity of H_2 through

zeolite crystals at 298 K) can be estimated from the slope of the linear fitting of the plot of equation (5-28). $D_{H_2,0}$ is found to be on the order of 10^{-8} (m^2 s^{-1}), which is consistent with literature values for zeolite minerals with pore sizes similar to clinoptilolite. De Lara et al.[81] have reported diffusivity of H_2 to be equal to 3×10^{-8} (m^2 s^{-1}) in zeolite A at room temperature. In MFI membranes Sandström et al.[82] have obtained the value of 3.6×10^{-8} (m^2 s^{-1}) for diffusivity of H_2 at room temperature.

5.1.4- Energy-dispersive X-ray spectroscopy

The elemental surface analysis of each sample performed by EDX is shown in Table 5.4. M2 has a Si/Al ratio of ~4 which is lower than that of M1 (Si/Al ~ 5.5). Clinoptilolite generally has a Si/Al ratio between 4.2-5.3.[35] This higher value of Si/Al ratio for M1 could be associated with a larger amount of SiO_2 impurities and smaller zeolite content in this membrane. CO_2 isotherms measured for these materials (Figure 5.4) show that CO_2 adsorption capacity for M2 is nearly twice as high as for M1 at room temperature. This infers a higher clinoptilolite content in M2 compared to M1. CO_2 molecules have strong interactions with most zeolite frameworks. Consequently, the CO_2 adsorption capacity (mol/kg) of the membrane material can be associated with its clinoptilolite content[83].

Table 5.4. Chemical composition (normalized wt.%) of the membrane sample, determined by energy dispersive X-ray analysis

Sample	M1	M2
Fe	3.25	8.24
Ca	6.02	7.04
Mg	0.78	1.76
Al	8.83	11.47
Si	47.95	45.55
K	2.88	2.88
Na	0.68	1.96
Cl	0.00	0.00
Ti	0.32	0.64
O	29.29	20.64

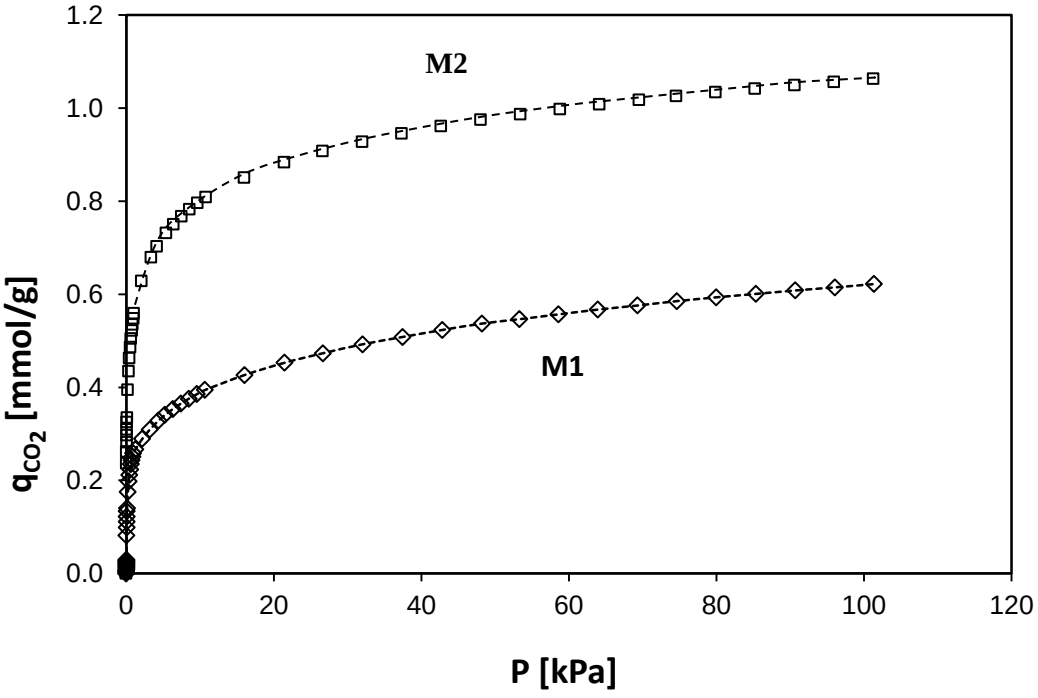

Figure 5.4. CO_2 isotherms for M1 and M2 at 298 K.

M1 has higher permeability than M2 because the mass transport is less restricted due to the higher density of inter-crystalline channels in the membrane. This is consistent with the lower zeolite content of M1 compared to M2, and the lower bulk density of the original mineral sample. The key observations of the characterization of membranes M1 and M2 are summarized in Table 5.5.

Table 5.5. Summary of M1 and M2 membranes characterization

Observation	Characteristic	M1	M2
Lower Si/Al ratio → Higher CO_2 adsorption capacity	Higher zeolite content		✓
Higher selectivity at lower pressures → Higher bulk density → Lower permeability	Less non-zeolite area / higher tortuosity		✓
Higher selectivity at higher Pressures →	Smaller average defect size	✓	

5.2- Simulated permeation fluxes of single component H_2 and CO_2

5.2.1- Effect of temperature

Figures 5.5 and 5.6 show H_2 and CO_2 permeances as functions of temperature when both feed and permeate pressures are equal to 101.35 kPa. The driving force for permeation is associated with the partial pressure drop of either H_2 or CO_2. The H_2 or CO_2 fluxes through the membrane represent only a combination of zeolite and Knudsen contributions because there is no viscous flow as there is no total pressure difference. Permeance associated with Knudsen diffusion decreases as the temperature rises[62,87]. Zeolitic permeance increases with temperature as $E_i^D + \Delta H_i > 0$.

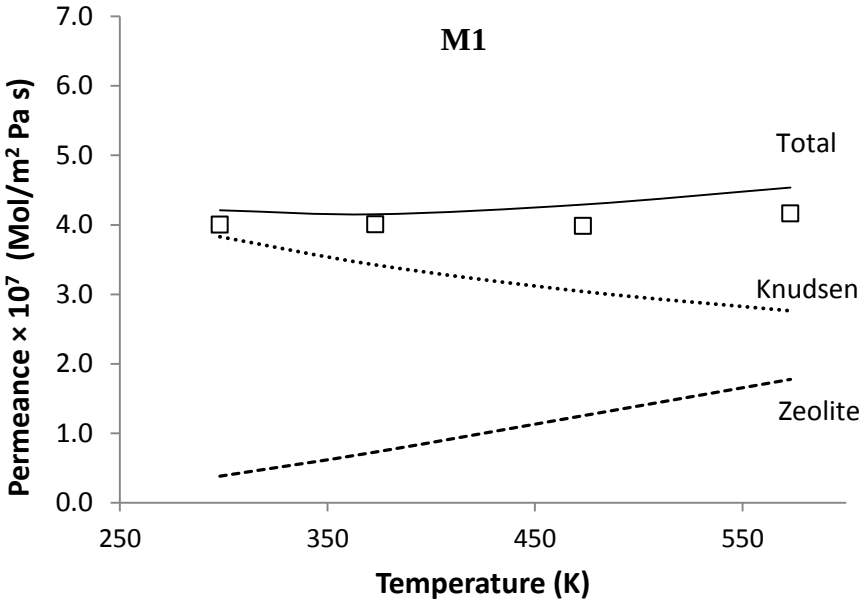

Figure 5.5. Contribution of the transport mechanisms to total H_2 permeance as a function of temperature across membrane M1. Feed and permeate pressures are equal to 101.3 kPa. The square represents experimental measurements.

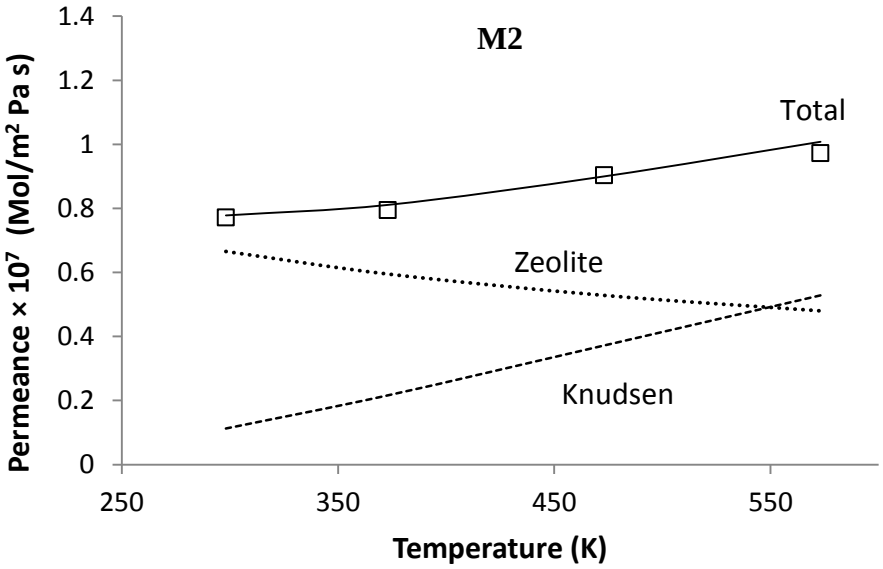

Figure 5.6. Contribution of the transport mechanisms to total H_2 permeance as a function of temperature across membrane M2. Feed and permeate pressures are equal to 101.3 kPa. The square represents experimental measurements.

Permeances through membrane M2 increased slightly with temperature compared to M1 (Figures 5.6 and 5.7). The H_2 permeance for M2 increased ~ 25% when temperature rose from 298K to 550K. However, the permeance through M1 only increased ~5% in the same temperature range. This can be attributed to the larger contribution of zeolite flux to the total flux across M2 when the temperature rises. These results are consistent with the higher zeolite content of M2 and are further supported by CO_2 isotherms (Section 5.1.4). CO_2 permeation shows similar behavior with an increase in temperature. The corresponding modeling figures for CO_2 are shown in figures 5.7 and 5.8.

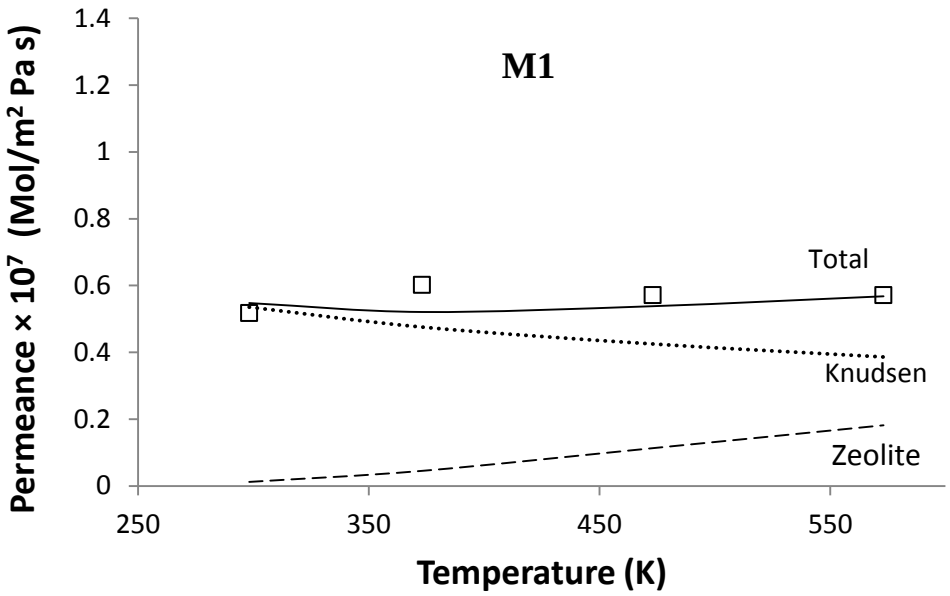

Figure 5.7. Contribution of the transport mechanisms to total CO_2 permeance as a function of temperature across M1. The square represents experimental measurements

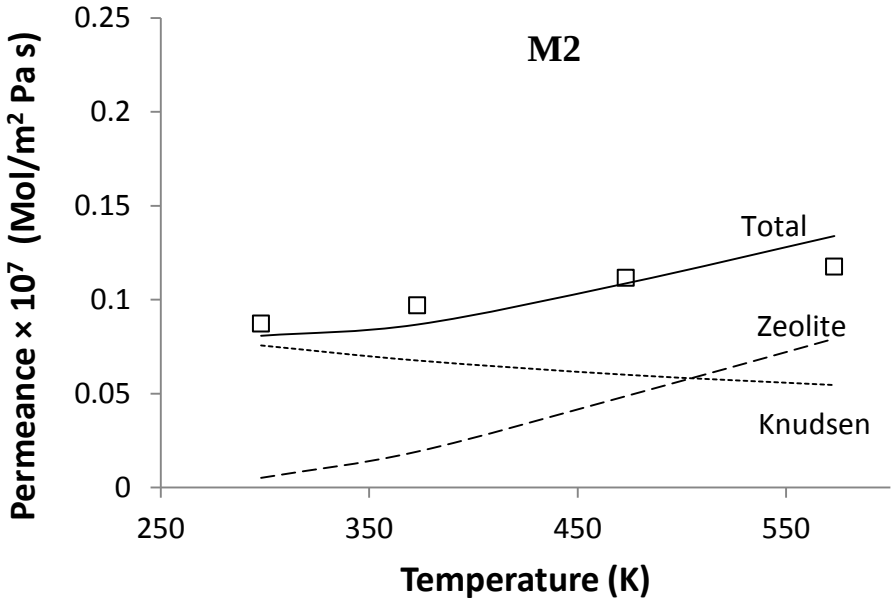

Figure 5.8. Contribution of the transport mechanisms to total CO_2 permeance as a function of temperature across M2. The square represents experimental measurements.

Figure 5.9 shows H_2 permeance as a function of temperature for the M2 membrane at 34.5 kPa pressure drop. At these pressure conditions, in addition to the zeolitic and Knudsen fluxes, viscous transport also contributes to the total H_2 flux. Similar to Knudsen permeance, the permeance associated with viscous flux decreases with temperature. As the temperature increases, a higher fraction of H_2 total flux passes through the zeolite crystals.

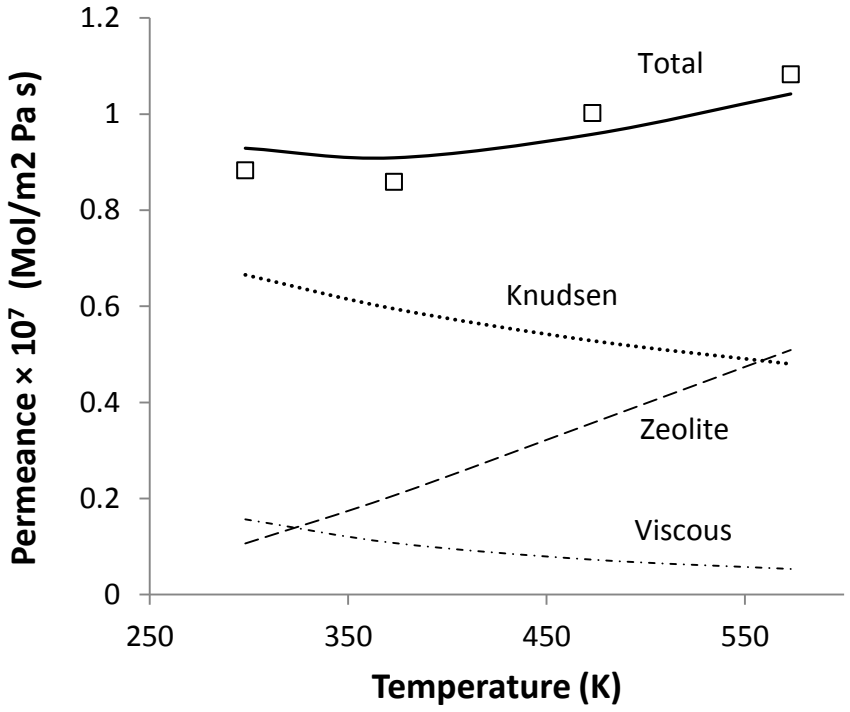

Figure 5.9. Dependence of H_2 permeance on temperature across M2. Contribution to total H_2 permeance from: a) different transport mechanisms, and b) selective and non-selective fractions at feed pressure of 135.8 kPa and permeate pressure of 101.3 kPa.

As shown in Figure 5.10, the selective fraction of H_2 permeance able to provide separation selectivity (either molecular sieve or Knudsen), increases with temperature. On the contrary, the non-selective fraction related to the flux through

relatively large non-zeolite pores (viscous flux) decreases with temperature. This membrane behavior can be advantageous for potential applications in the hydrogen separation industry where the process temperatures can reach higher than 523 K[68].

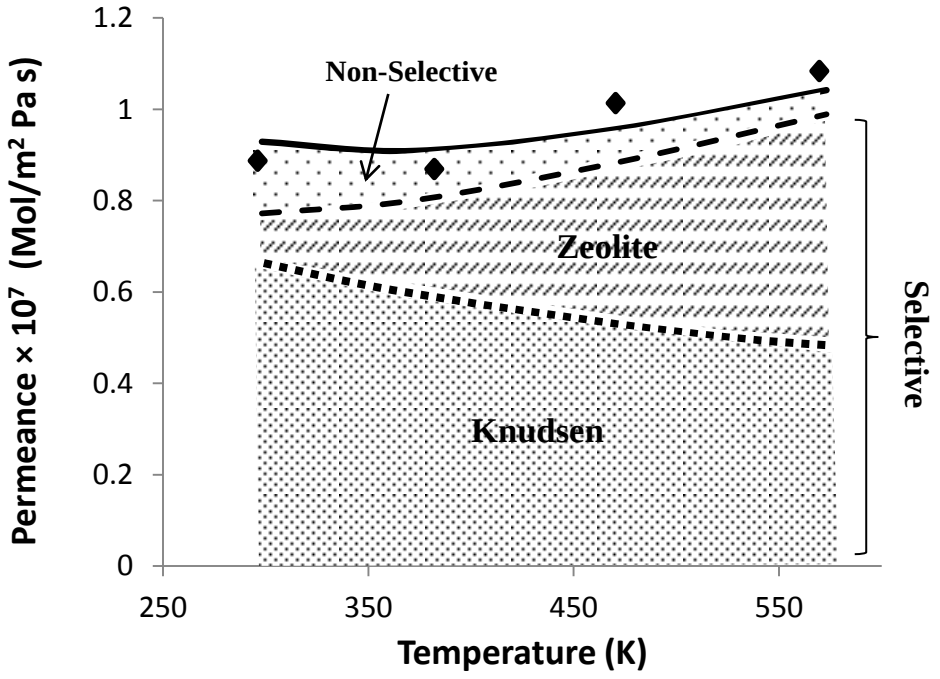

Figure 5.10. Dependence of H_2 permeance on temperature across M2. Contribution to total H_2 permeance from: a) different transport mechanisms, and b) selective and non-selective fractions at feed pressure of 135.8 kPa and permeate pressure of 101.3 kPa.

5.2.2- Effect of pressure

Simulated H_2 and CO_2 permeances as a function of temperature at different feed pressure values along with the experimental data are shown in Figures 5.11 and 5.12. As both temperature and pressure increased, the mathematical model closely

described the permeance behaviors for the membranes. The H_2 and CO_2 permeances through the membranes increased as the feed pressure rose. This is due to the higher viscous flux contribution through the relatively large non-zeolite pores. The permeance associated with the Knudsen flux remains constant as pressure increases. However, permeance related to the zeolitic flux is either constant or slightly decreases with pressure. CO_2 permeance is lower than H_2. The influence of pressure on the total permeance is slightly visible at higher temperatures for both CO_2 and H_2. This can be explained by less viscous flux contribution as temperature rises. At higher temperatures, the zeolite flux and the Knudsen transport dominate (Figure 5.10).

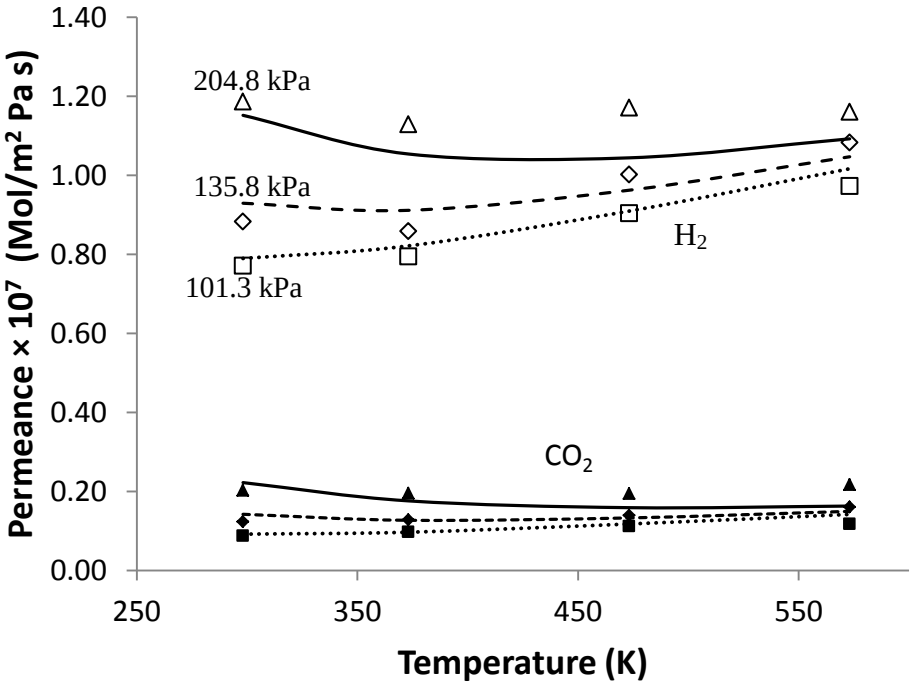

Figure 5.11. H_2 and CO_2 permeance for membrane M2 as a function of temperature at different feed pressures.

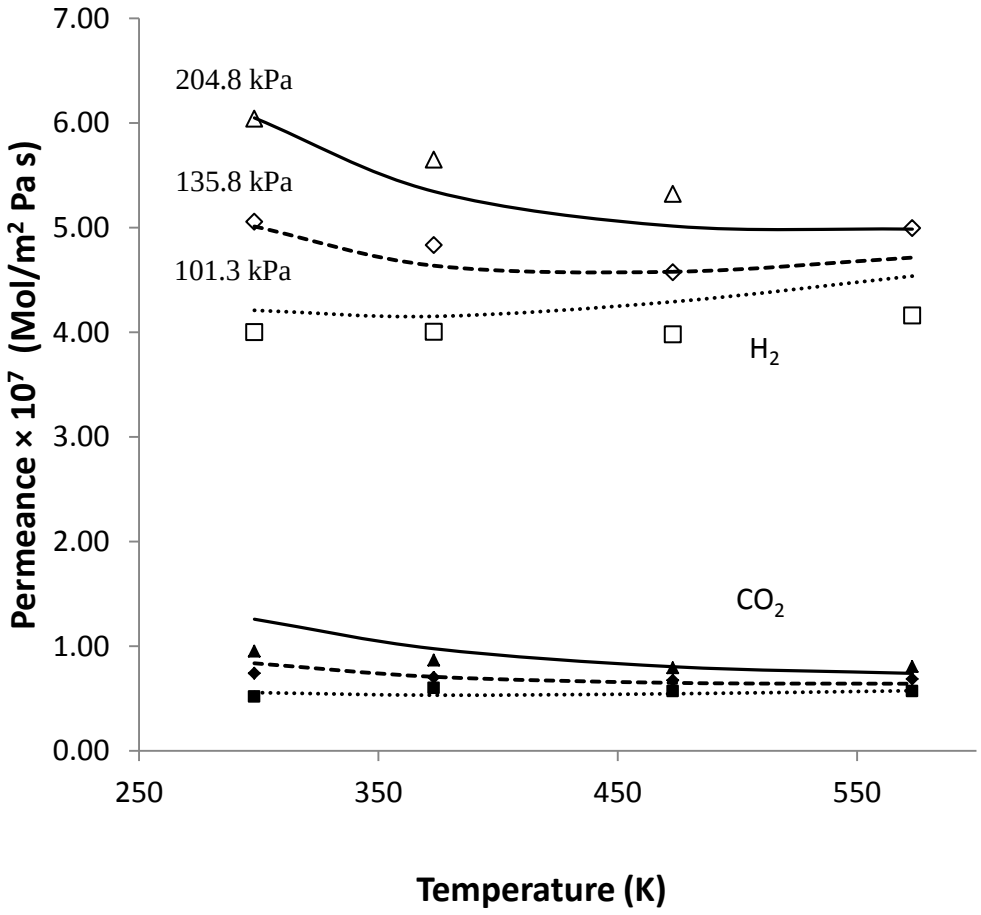

Figure 5.12. H_2 and CO_2 permeance for membrane M1 as a function of temperature at different feed pressures.

Chapter 6. Conclusion and Recommendations

Current environmental problems and high energy demand have created a need to search for cleaner fuels. Hydrogen has been proposed as a clean zero emission fuel. Moreover, Hydrogen is the main feedstock in many petrochemical industries. The problem with hydrogen production is that it does not exist in a free molecule form and needs to be separated from its mixture with other gases and impurities. Membrane-based processes have the potential to overcome the limitations of the conventional hydrogen separation techniques such as high energy consumption and environmental concerns.

Geomorphic natural zeolite membranes have shown promise in H_2 and CO_2 separation for the purification of hydrogen. H_2 and CO_2 permeation measurements through natural clinoptilolite based membranes were performed at temperatures ranging from 298 K to 573 K, and feed pressures from 101.3 kPa to 202.7 kPa. Membranes were characterized based on simple comparative parameters. The results from these analyses were consistent with the adsorption isotherms and experimental ideal permeance selectivities. A model based on the combination of zeolitic, Knudsen and viscous transports was used to fit the H_2 and CO_2 permeance data. Temperature and pressure effects were studied in different membranes. A comparison of membranes from different mineral samples (M1 and M2) showed different zeolite flux contributions. Membrane M2, with a higher zeolite flux fraction, showed a lower permeability at room temperature than M1,

but it had a steeper increase of H_2 permeance as temperature increased. Membrane M2 had higher bulk density and larger CO_2 adsorption capacity compared to M1. Total permeance increased with the increase of feed pressure especially at lower temperatures. The increase was less apparent at high temperatures. This is due to the larger contribution of the selective flux fractions (zeolite and Knudsen) compared to the non-selective flux fraction (viscous flux) at higher temperatures.

Simulation of membrane permeance is useful for the analysis of experimental observation. This characterization technique can be advantageous in development and optimization of natural zeolite membranes for industrial applications, especially in high-temperature hydrogen separation industries. The work presented in this thesis can be extended by improving the natural zeolite membranes used in this study and analyzing the effect of membrane modification on membrane performance. Comparing more membranes made from different natural zeolite minerals to identify the best deposit is recommended. One other area that has the potential for future improvements is the modeling and simulation of multicomponent permeance measurements in order to compare it with the simulation of single gas permeance through natural zeolite membranes.

References

(1) International Energy Outlook 2010, U.S. Energy Information Administration, Available online at: www.eia.gov/oiaf/ieo/index.html. **July 2010**.

(2) Adhikari, S.; Fernando, S. Hydrogen membrane separation techniques. *Industrial and Engineering Chemistry Research* **2006**, *45*, 875-881.

(3) Dong, J.; Lin, Y. S.; Kanezashi, M.; Tang, Z. Microporous inorganic membranes for high temperature hydrogen purification. *J. Appl. Phys.* **2008**, *104*.

(4) Separation technology R&D needs for hydrogen production in the chemical and petrochemical industries prepared for U.S. Department of Energy Office of Energy Efficiency and Renewable Energy's Industrial Technologies Program. **2005**.

(5) Ockwig, N. W.; Nenoff, T. M. Membranes for hydrogen separation. *Chem. Rev.* **2007**, *107*, 4078-4110.

(6) Aberg, C. M. Membranes for hydrogen purification: An important step toward a hydrogen-based economy. *MRS Bull* **2006**, *31*, 735-741.

(7) Mueller-Langer, F.; Tzimas, E.; Kaltschmitt, M.; Peteves, S. Techno-economic assessment of hydrogen production processes for the hydrogen economy for the short and medium term. *Int J Hydrogen Energy* **2007**, *32*, 3797-3810.

(8) Nenoff, T. M. In *In Defect-free thin film zeolite membranes for hydrogen separation and isolation , in: DOE/H_2. Annual Review Meeting;* 2003; .

(9) Thomas, S.; Zalbowitz, M.; Cruz, J. Fuel Cells—Green Power. **1999**.

(10) Meyers, R. A. In *Handbook of Petroleum Refining Processes;* McGraw-Hill: New York, 2004; .

(11) Skarstrom, C. W. U.S. Patent No. 2,944,627, 1960.

(12) Prausnitz, J. M.; Lichtenthaler, R. N.; Azevedo, E. G. In *Molecular Thermodynamics of Fluid-Phase Equilibria;* Prentice Hall: New York, 1999; .

(13) Welk, M. E.; Nenoff, T. M.; Bonhomme, F. In *Studies in Surfaces and Catalysis;* Elsevier B.V.: New York, 2004; Vol. 154.

(14) Xu, X.; Yang, W.; Liu, J.; Lin, L. Synthesis of NaA zeolite membrane by microwave heating. *Separation and Purification Technology* **2001**, *25*, 241-249.

(15) Coronas, J.; Falconer, J. L.; Noble, R. D. Characterization and Permeation Properties of ZSM-5 Tubular Membranes. *AICHE J.* **1997**, *43*, 1797-1812.

(16) Yan, Y.; Davis, M. E.; Gavalas, G. R. Preparation of zeolite ZSM-5 membranes by in-situ crystallization on porous α-Al2O3. *Industrial and Engineering Chemistry Research* **1995**, *34*, 1652-1661.

(17) Coronas, J.; Santamaría, J. Separations using zeolite membranes. *Sep. Purif. Methods* **1999**, *28*, 127-177.

(18) van Bekkum, H.; Geus, E. R.; Kouwenhoven, H. W. Supported zeolite systems and applications. *Studies in Surface Science and Catalysis* **1994**, *85*, 509-542.

(19) Kusakabe, K.; Kuroda, T.; Uchino, K.; Hasegawa, Y.; Morooka, S. Gas permeation properties of ion-exchanged faujasite-type zeolite membranes. *AICHE J.* **1999**, *45*, 1220-1226.

(20) Aoki, K.; Kusakabe, K.; Morooka, S. Gas permeation properties of A-type zeolite membrane formed on porous substrate by hydrothermal synthesis. *J. Membr. Sci.* **1998**, *141*, 197-205.

(21) Burggraaf, A. J.; Vroon, Z. A. E. P.; Keizer, K.; Verweij, H. Permeation of single gases in thin zeolite MFI membranes. *J. Membr. Sci.* **1998**, *144*, 77-86.

(22) Gavalas, G. R. In *Zeolite Membranes for Gas and Liquid Separations;* Yampolskii, Y., Pinnau, I. and Freeman, B. D., Eds.; Materials Science of Membranes for Gas and Vapor Separation; John Wiley & Sons, Ltd.: New York, 2006; pp 307-336.

(23) Caro, J.; Noack, M. Zeolite membranes - Recent developments and progress. *Microporous and Mesoporous Materials* **2008**, *115*, 215-233.

(24) White, J. C.; Dutta, P. K.; Shqau, K.; Verweij, H. Synthesis of ultrathin zeolite y membranes and their application for separation of carbon dioxide and nitrogen gases. *Langmuir* **2010**, *26*, 10287-10293.

(25) Snyder, M. A.; Tsapatsis, M. Hierarchical nanomanufacturing: From shaped zeolite nanoparticles to high-performance separation membranes. *Angewandte Chemie - International Edition* **2007**, *46*, 7560-7573.

(26) Lin, Y. S.; Kumakiri, I.; Nair, B. N.; Alsyouri, H. Microporous inorganic membranes. *Sep. Purif. Methods* **2002**, *31*.

(27) An, W.; Swenson, P.; Wu, L.; Waller, T.; Ku, A.; Kuznicki, S. M. Selective separation of hydrogen from C1/C2 hydrocarbons and CO_2 through dense natural zeolite membranes. *J. Membr. Sci.* **2011**, *369*, 414-419.

(28) Wellington, J. M.; Ku, A. Y. Opportunities for membranes in sustainable energy. *J. Membr. Sci.* **2011**, *373*, 1-4.

(29) Merkel, T. C.; Lin, H.; Wei, X.; Baker, R. Power plant post-combustion carbon dioxide capture: An opportunity for membranes. *J. Membr. Sci.* **2010**, *359*, 126-139.

(30) Devi, D. A.; Smitha, B.; Sridhar, S.; Aminabhavi, T. M. Pervaporation separation of isopropanol/water mixtures through crosslinked chitosan membranes. *J. Membr. Sci.* **2005**, *262*, 91-99.

(31) Mendes, D.; Chibante, V.; Zheng, J. -.; Tosti, S.; Borgognoni, F.; Mendes, A.; Madeira, L. M. Enhancing the production of hydrogen via water-gas shift reaction using Pd-based membrane reactors. *Int J Hydrogen Energy* **2010**, *35*, 12596-12608.

(32) Baker, R. W. Future directions of membrane gas separation technology. *Industrial and Engineering Chemistry Research* **2002**, *41*, 1393-1411.

(33) Perry, J. D.; Nagai, K.; Koros, W. J. Polymer membranes for hydrogen separations. *MRS Bull* **2006**, *31*, 745-749.

(34) Staudt-Bickel, C.; J. Koros, W. Improvement of CO_2/CH_4 separation characteristics of polyimides by chemical crosslinking. *J. Membr. Sci.* **1999**, *155*, 145-154.

(35) D.W. Breck In *Zeolite Molecular Sieves – Structure, Chemistry, and Use;* John Wiley & Sons, Ltd: New York, 1974; .

(36) Baerlocher, C.; McCusker, L. B.; Olson, D. H. In *Atlas of Zeolite Framework Types;* Elsevier: Amsterdam, 2007; .

(37) Kuznicki, S. M. CHE 584 Class Notes, Molecular Sieve Technology, University of Alberta, Winter 2010.

(38) Kanezashi, M.; O'Brien-Abraham, J.; Lin, Y. S.; Suzuki, K. Gas permeation through DDR-type zeolite membranes at high temperatures. *AICHE J.* **2008**, *54*, 1478-1486.

(39) Gu, Y.; Hacarlioglu, P.; Oyama, S. T. Hydrothermally stable silica-alumina composite membranes for hydrogen separation. *J. Membr. Sci.* **2008**, *310*, 28-37.

(40) Zheng, Z.; Hall, A. S.; Guliants, V. V. Synthesis, characterization and modification of DDR membranes grown on α-alumina supports. *J. Mater. Sci.* **2008**, 1-4.

(41) Tanaka, H.; Yamasaki, N.; Muratani, M.; Hino, R. Structure and formation process of (K,Na)-clinoptilolite. *Mater. Res. Bull.* **2003**, *38*, 713-722.

(42) Caro, J.; Noack, M. Zeolite membranes – Recent developments and progress. *Microporous and Mesoporous Materials* **2008**, *115*, 215-233.

(43) Caro, J.; Noack, M.; Kölsch, P.; Schäfer, R. Zeolite membranes - state of their development and perspective. *Microporous and Mesoporous Materials* **2000**, *38*, 3-24.

(44) Dong, J.; Lin, Y. S.; Liu, W. Multicomponent hydrogen/hydrocarbon separation by MFI-type zeolite membranes. *AICHE J.* **2000**, *46*, 1957-1966.

(45) Carreon, M. A.; Li, S.; Falconer, J. L.; Noble, R. D. Alumina-supported SAPO-34 membranes for CO_2/CH_4 separation. *J. Am. Chem. Soc.* **2008**, *130*, 5412-5413.

(46) Hasegawa, Y.; Watanabe, K.; Kusakabe, K.; Morooka, S. The separation of CO_2 using Y-type zeolite membranes ion-exchanged with alkali metal cations. *Separation and Purification Technology* **2001**, *22-23*, 319-325.

(47) Tavolaro, A.; Drioli, E. Zeolite membranes. *Adv Mater* **1999**, *11*, 975-996.

(48) Kita, H.; Fuchida, K.; Horita, T.; Asamura, H.; Okamoto, K. Preparation of Faujasite membranes and their permeation properties. *Separation and Purification Technology* **2001**, *25*, 261-268.

(49) Maesen, T.; Marcus, B. The zeolite scene - An overview. *Studies in Surface Science and Catalysis* **2001**, *137*, 1-9.

(50) Gu, X.; Dong, J.; Nenoff, T. M.; Ozokwelu, D. E. Separation of p-Xylene from Multicomponent Vapor Mixtures using Tubular MFI Zeolite Membranes. *Studies in Surface Science and Catalysis* **2007**, *170*, 949-954.

(51) Pina, M. P.; Mallada, R.; Arruebo, M.; Urbiztondo, M.; Navascués, N.; De La Iglesia, O.; Santamaria, J. Zeolite films and membranes. Emerging applications. *Microporous and Mesoporous Materials* **2011**, *144*, 19-27.

(52) McLeary, E. E.; Jansen, J. C. Basic Views on the Preparation of Porous Ceramic Membrane Layers: A Comparison Between Amorphous and Crystalline Layers, Leading to a New Method for the Preparation of Microporous Continuous Layers. *Topics in Catalysis* **2004**, *29*, 85-92.

(53) Junaid, A. S. M.; Rahman, M.; Yin, H.; McCaffrey, W. C.; Kuznicki, S. M. Natural zeolites for oilsands bitumen cracking: Structure and acidity. *Microporous and Mesoporous Materials* **2011**, *144*, 148-157.

(54) Ackley, M. W.; Rege, S. U.; Saxena, H. Application of natural zeolites in the purification and separation of gases. *Microporous and Mesoporous Materials* **2003**, *61*, 25-42.

(55) Ackley, M. W.; Giese, R. F.; Yang, R. T. Clinoptilolite: Untapped potential for kinetics gas separations. *Zeolites* **1992**, *12*, 780-788.

(56) Haggerty, G. M.; Bowman, R. S. Sorption of chromate and other inorganic anions by organo-zeolite. *Environmental Science and Technology* **1994**, *28*, 452-458.

(57) Aguilar-Armenta, G.; Romero-Pérez, A. Adsorption of C_2H_4, C_2H_6 and CO_2 on cation-exchanged clinoptilolite. *Adsorption Science and Technology* **2009**, *27*, 523-536.

(58) Aguilar-Armenta, G.; Hernandez-Ramirez, G.; Flores-Loyola, E.; Ugarte-Castaneda, A.; Silva-Gonzalez, R.; Tabares-Munoz, C.; Jimenez-Lopez, A.; Rodriguez-Castellon, E. Adsorption kinetics of CO_2, O_2, N_2, and CH_4 in cation-exchanged clinoptilolite. *J Phys Chem B* **2001**, *105*, 1313-1319.

(59) Günay, A.; Arslankaya, E.; Tosun, I. Lead removal from aqueous solution by natural and pretreated clinoptilolite: Adsorption equilibrium and kinetics. *J. Hazard. Mater.* **2007**, *146*, 362-371.

(60) Inglezakis, V. J.; Loizidou, M. D.; Grigoropoulou, H. P. Ion exchange of Pb2+, Cu2+, Fe3+, and Cr3+ on natural clinoptilolite: Selectivity determination and influence of acidity on metal uptake. *J. Colloid Interface Sci.* **2003**, *261*, 49-54.

(61) Hanebuth, M.; Dittmeyer, R.; Mabande, G. T. P.; Schwieger, W. On the combination of different transport mechanisms for the simulation of steady-state mass transfer through composite systems using H_2

/SF_6 permeation through stainless steel supported silicalite-1 membranes as a model system. *Catalysis Today* **2005**, *104*, 352-359.

(62) Tarditi, A. M.; Lombardo, E. A.; Avila, A. M. Xylene permeation transport through composite Ba-ZSM-5/SS tubular membranes: Modeling the steady-state permeation. *Industrial and Engineering Chemistry Research* **2008**, *47*, 2377-2385.

(63) Marković, A.; Stoltenberg, D.; Enke, D.; Schlünder, E. -.; Seidel-Morgenstern, A. Gas permeation through porous glass membranes. Part I. Mesoporous glasses-Effect of pore diameter and surface properties. *J. Membr. Sci.* **2009**, *336*, 17-31.

(64) Marković, A.; Stoltenberg, D.; Enke, D.; Schlünder, E. -.; Seidel-Morgenstern, A. Gas permeation through porous glass membranes. Part II: Transition regime between Knudsen and configurational diffusion. *J. Membr. Sci.* **2009**, *336*, 32-41.

(65) Colin, S. Rarefaction and compressibility effects on steady and transient gas flows in microchannels. *Microfluid Nanofluid* **2005**, *1*, 268-279.

(66) Avila, A. M.; Sedran, U. Separation of ternary hydrocarbon mixtures on Y zeolite membranes. *Chem. Eng. J.* **2009**, *146*, 338-344.

(67) Krishna, R.; Baur, R. Modelling issues in zeolite based separation processes. *Separation and Purification Technology* **2003**, *33*, 213-254.

(68) Krishna, R. Describing the diffusion of guest molecules inside porous structures. *Journal of Physical Chemistry C* **2009**, *113*, 19756-19781.

(69) Kapteijn, F.; Van De Graaf, J. M.; Moulijn, J. A. One-component permeation maximum diagnostic tool for silicate-1 membrane. *AICHE J.* **2000**, *46*, 1096-1100.

(70) Lito, P. F.; Zhou, C. F.; Santiago, A. S.; Rodrigues, A. E.; Rocha, J.; Lin, Z.; Silva, C. M. Modelling gas permeation through new microporous titanosilicate AM-3 membranes. *Chem. Eng. J.* **2010**, *165*, 395-404.

(71) E.A. Mason, A. P. M. In *Gas Transport in Porous Media: The Dusty-gas Model;* Elsevier: Amsterdam, 1983; .

(72) Thomas, S.; Schäfer, R.; Caro, J.; Seidel-Morgenstern, A. Investigation of mass transfer through inorganic membranes with several layers. *Catalysis Today* **2001**, *67*, 205-216.

(73) Krishna, R.; Wesselingh, J. A. Review article number 50: The Maxwell-Stefan approach to mass tranfer. *Chemical Engineering Science* **1997**, *52*, 861-911.

(74) Crane Company, *Flow of fluids through valves, fittings, and pipe;* Technical Paper No. 410; *1988*.

(75) Chemical Rubber Company, *CRC Handbook of Chemistry and Physics;* Weast, R. C., Ed.; Boca Raton: Florida, 1984.

(76) Čapek, P.; Hejtmánek, V.; Šolcováa, O. Permeation of gases in industrial porous catalysts. *Chem. Eng. J.* **2001**, *81*, 281-285.

(77) Miachon, S.; Ciavarella, P.; van Dyk, L.; Kumakiri, I.; Fiaty, K.; Schuurman, Y.; Dalmon, J. -. Nanocomposite MFI-alumina membranes via pore-plugging synthesis: Specific transport and separation properties. *J. Membr. Sci.* **2007**, *298*, 71-79.

(78) Lin, Y. S.; Burggraaf, A. J. Experimental studies on pore size change of porous ceramic membranes after modification. *J. Membr. Sci.* **1993**, *79*, 65-82.

(79) Cao, G. Z.; Meijernik, J.; Brinkman, H. W.; Burggraaf, A. J. Permporometry study on the size distribution of active pores in porous ceramic membranes. *J. Membr. Sci.* **1993**, *83*, 221-235.

(80) Kärger, J.; Caro, J.; Cool, P.; Coppens, M. -.; Jones, D.; Kapteijn, F.; Rodríguez-Reinoso, F.; Stöcker, M.; Theodorou, D.; Vansant, E. F.; Weitkamp, J. Benefit of microscopic diffusion measurement for the characterization of nanoporous materials. *Chemical Engineering and Technology* **2009**, *32*, 1494-1511.

(81) Cohen De Lara, E.; Kahn, R. Diffusivity of hydrogen and methane molecules in A zeolites: Neutron scattering measurements and comparison. *Zeolites* **1992**, *12*, 256-260.

(82) Sandström, L.; Lindmark, J.; Hedlund, J. Separation of methanol and ethanol from synthesis gas using MFI membranes. *J. Membr. Sci.* **2010**, *360*, 265-275.

(83) Sirkecioğlu, A.; Erdem-Şenatalar, A. Estimation of the zeolite contents of tuffaceous samples from the bigadiç clinoptilolite deposit, Western Turkey. *Clays Clay Miner.* **1996**, *44*, 686-692.

(84) Areán, C. O.; Palomino, G. T.; Garrone, E.; Nachtigallová, D.; Nachtigall, P. Combined theoretical and FTIR spectroscopic studies on hydrogen adsorption on the zeolites Na-FER and K-FER. *J Phys Chem B* **2006**, *110*, 395-402.

(85) Gu, X.; Tang, Z.; Dong, J. On-stream modification of MFI zeolite membranes for enhancing hydrogen separation at high temperature. *Microporous and Mesoporous Materials* **2008**, *111*, 441-448.

(86) Kanezashi, M.; Lin, Y. S. Gas permeation and diffusion characteristics of mfi-type zeolite membranes at high temperatures. *Journal of Physical Chemistry C* **2009**, *113*, 3767-3774.

(87) Ritter, J. A.; Ebner, A. D. State-of-the-art adsorption and membrane separation processes for hydrogen production in the chemical and petrochemical industries. *Sep. Sci. Technol.* **2007**, *42*, 1123-1193.

(88) Xiao, J.; Wei, J. Diffusion mechanism of hydrocarbons in zeolites-I. Theory. *Chemical Engineering Science* **1992**, *47*, 1123-1141.

(89) Jareman, F.; Hedlund, J.; Creaser, D.; Sterte, J. Modelling of single gas permeation in real MFI membranes. *J. Membr. Sci.* **2004**, *236*, 81-89.

1